

2 Distribution Network Simulation

2.1 Introduction

Nowadays, power quality has become a great concern for both utilities and customers. With the increasing use of non-linear load being connected to the power system, more studies are needed. The problems associated with high harmonic content in the power system do not only result in the poor quality of supply but also the operation of the system will get affected. Harmonic currents are generated to a small extent and low distortion level by generation, transmission and distribution equipments and to a larger extent by the industrial and domestic loads [64]-[67].

Harmonic distortion in electric distribution system is increasingly growing due to the widespread use of single phase non-linear loads. Large concentration of these loads has the potential to raise harmonic voltages and currents in an electrical system to unacceptable high levels that can adversely affect the system. Hence there is need to study the impact of non-linear loads in the system. Harmonic survey of various typical non-linear single loads has been carried out. Yokogawa CW240 clamp on power analyzer is used for harmonic distortion measurement. Harmonic spectrum for each load is plotted. Finally total harmonic distortion is calculated and compared with the IEEE standard limits.

2.2 Harmonic Survey

Harmonic field measurement is done to verify the degree of severity of harmonic distortion due to domestic non-linear loads in the distribution network [68]. There are number of solid state controlled non-linear equipments are used for domestic application such as electronic fan regulator, personnel computer, printer, etc. These non-linear loads inject harmonic currents in the network thus distorting supply voltage. The major sources of harmonics are from the two categories of equipment: (a) industrial loads (b) domestic loads.

In carrying out harmonic measurement at Faculty of Electrical Engineering Department of C. K. Pithawalla Collage of Engineering and Technology, Surat, six types of domestic application were selected. All the measurements are made at 230 V using Yokogawa make clamp on type Power Analyzer (200 A, 600 V). Harmonic spectrum for each load is plotted showing magnitude of each harmonic frequency that makes up a distorted waveform. The magnitude of each harmonic frequency can be expressed as a percentage of fundamental. Total harmonic distortion is defined from harmonic spectrum as the ratio of the RMS sum of all harmonic frequencies to the RMS value of the fundamental.

Mathematically THD is expressed by the following equations [69]-[71]:

$$THD_V = \frac{\sqrt{\left(\sum_{h=2}^n V_h\right)^2}}{V_1} \quad (2.1)$$

$$THD_I = \frac{\sqrt{\left(\sum_{h=2}^n I_h\right)^2}}{I_1} \quad (2.2)$$

2.2.1 Industrial Loads

2.2.1.1 Laser machine

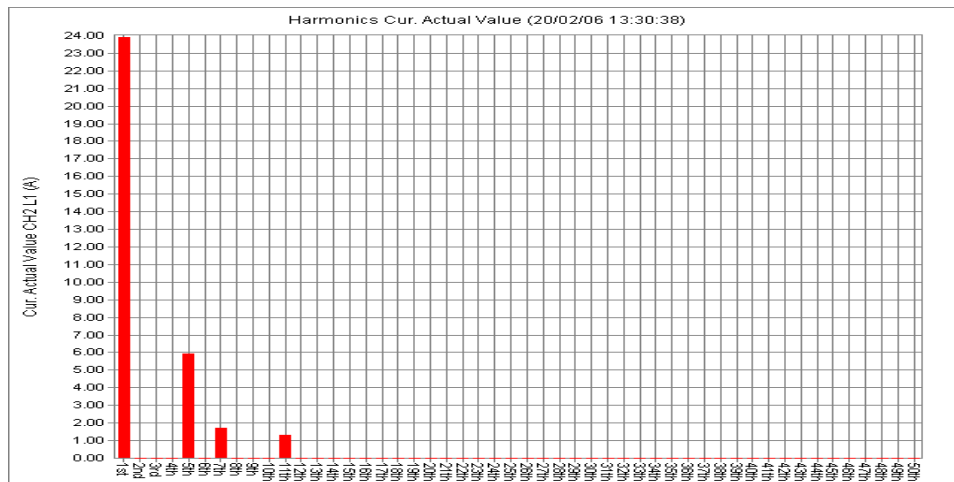


Figure 2.1 Current harmonic spectrums (Laser machine)

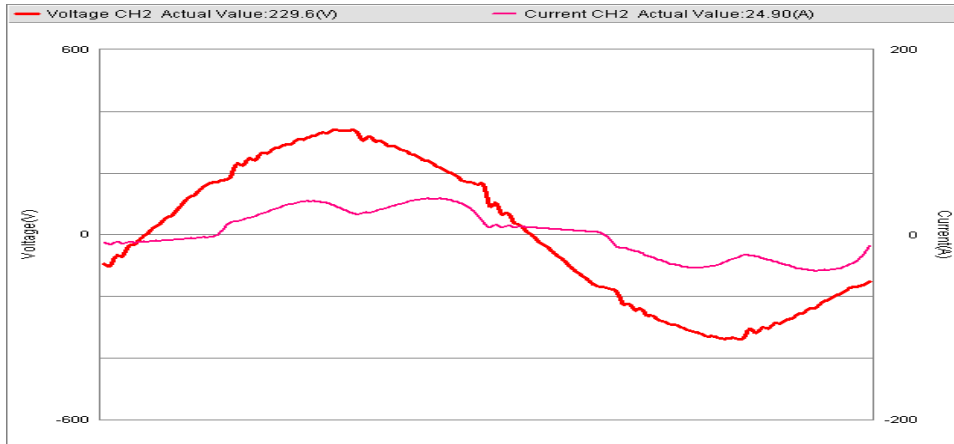


Figure 2.2 Voltage and current waveform (Laser machine)

2.2.1.2 Embroidery machine

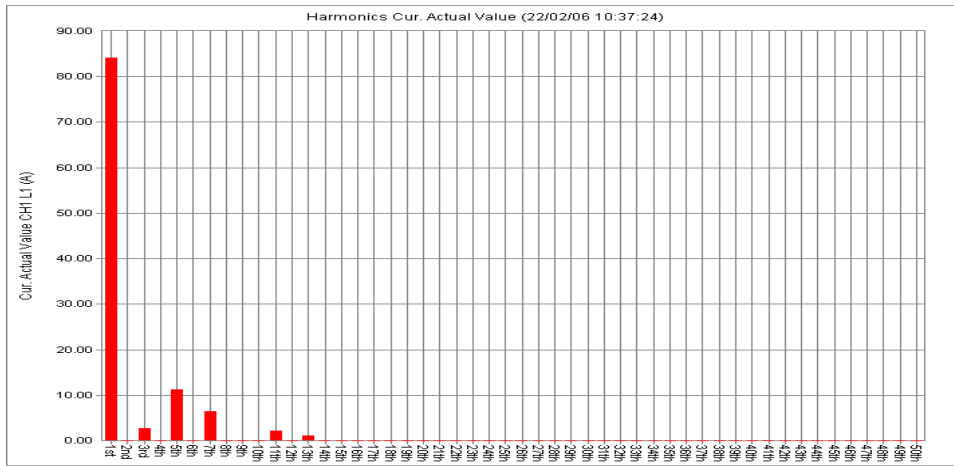


Figure 2.3 Current harmonic spectrum (Embroidery machine)

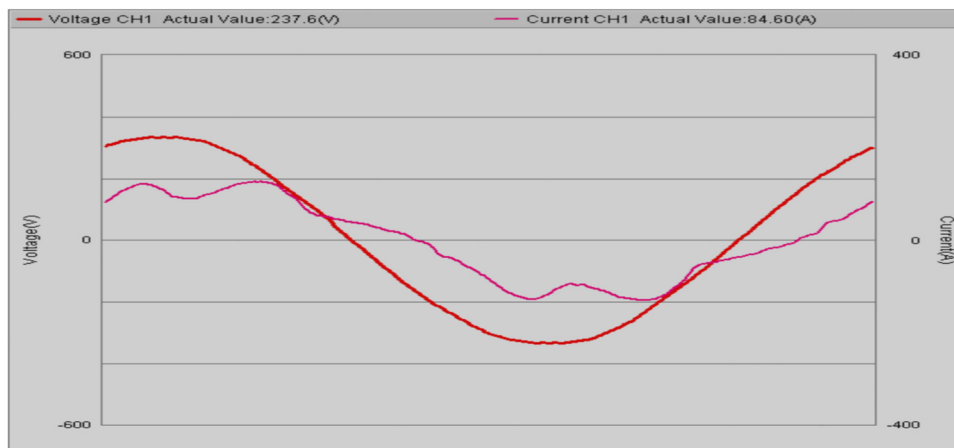


Figure 2.4 Voltage and current waveform (Embroidery machine)

2.2.1.3 Water Jet (textile industries)

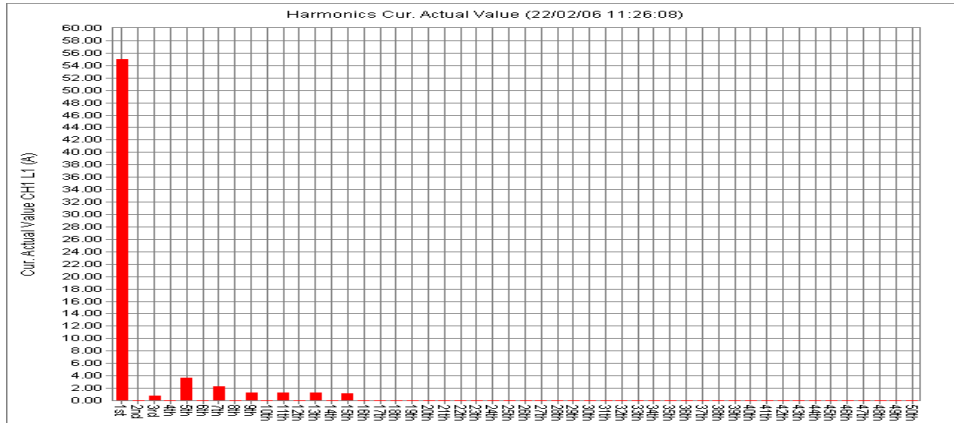


Figure 2.5 Current harmonic spectrums (Water jet)

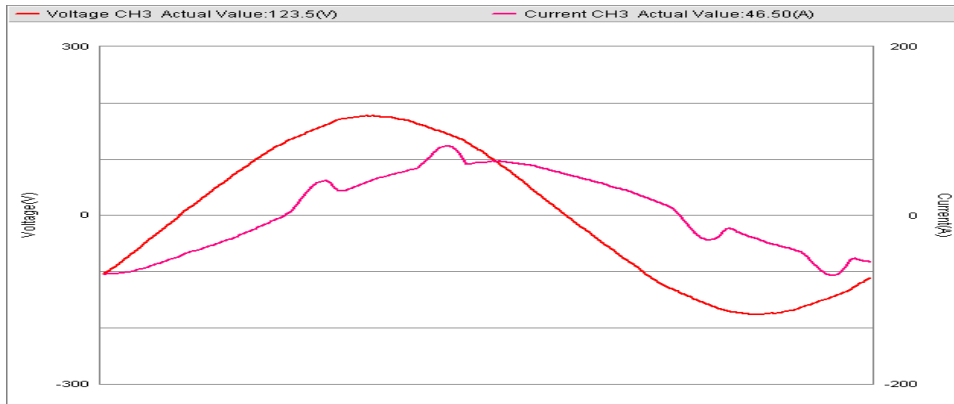


Figure 2.6 Voltage and current waveform (Water jet)

2.2.1.4 Electric Arc Furnace

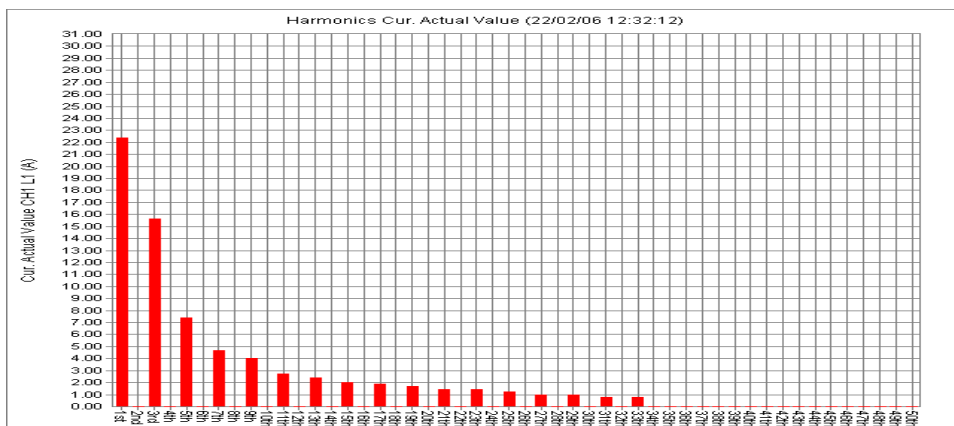


Figure 2.7 Current harmonic spectrums (EAF)

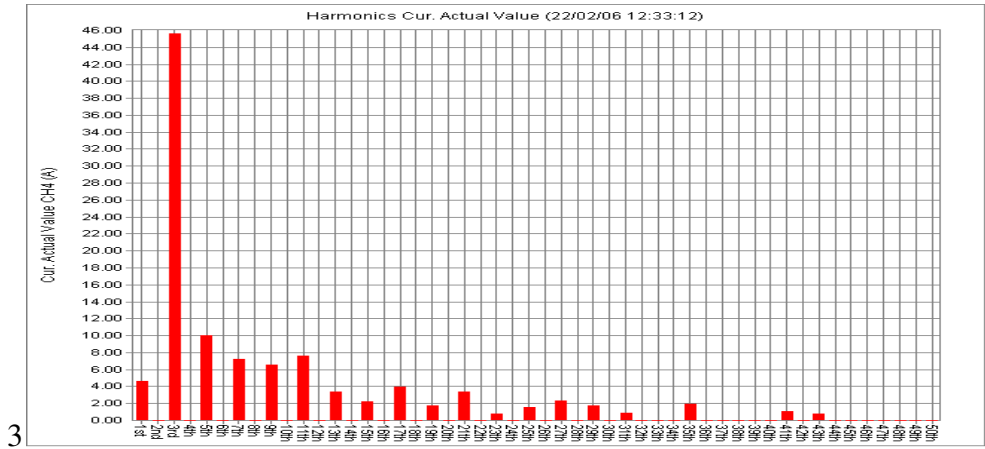


Figure 2.8 Current harmonic spectrums (EAF)

2.2.1.5 Uninterruptible power supply (UPS)

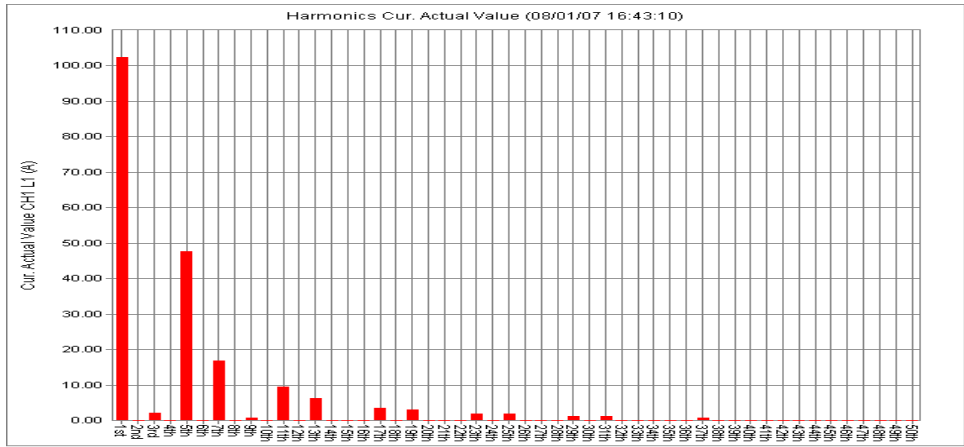


Figure 2.9 Current harmonic spectrums (UPS)

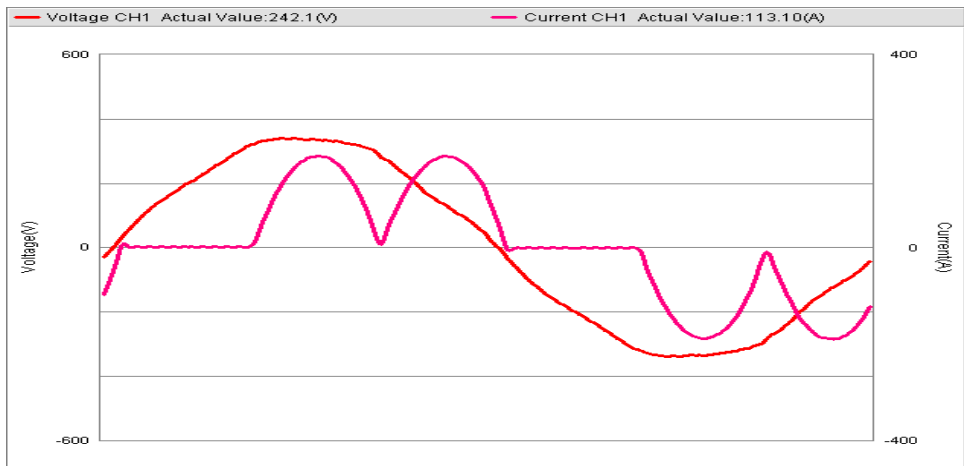


Figure 2.10 Voltage and current waveform (UPS)

2.2.1.6 Computer center

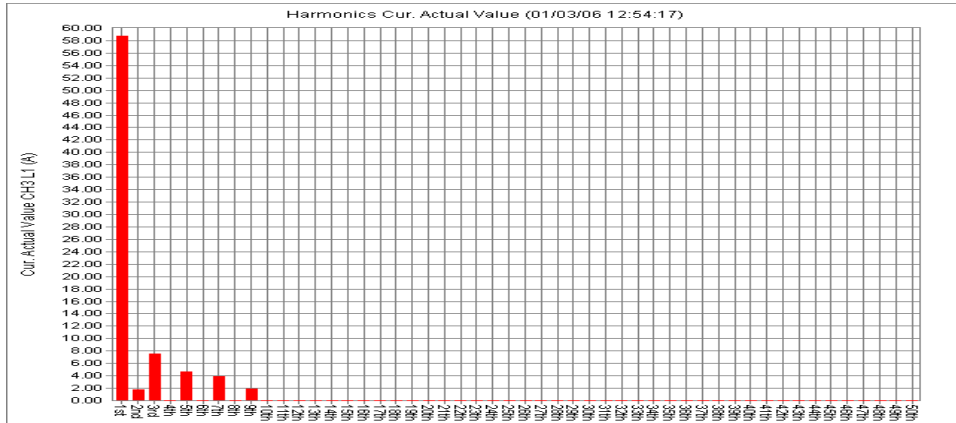


Figure 2.11 Current harmonic spectrums (Computer center)

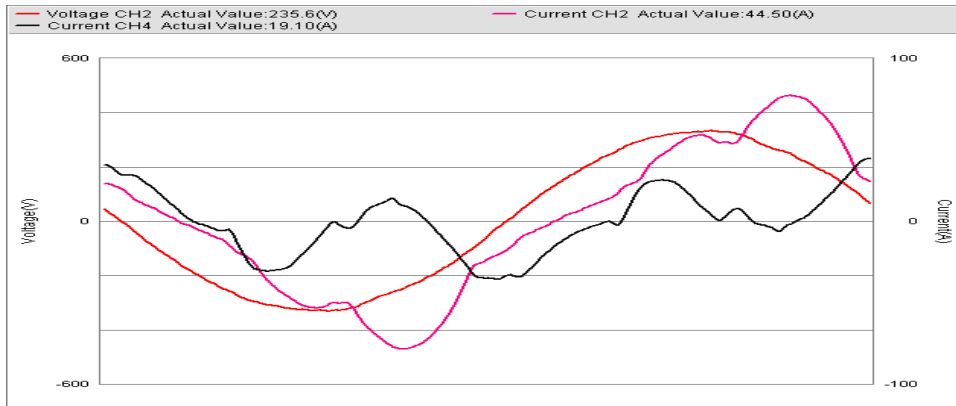


Figure 2.12 Voltage and current waveform (Computer center)

2.2.2 Domestic Loads

2.2.2.1 Electronic fan regulator

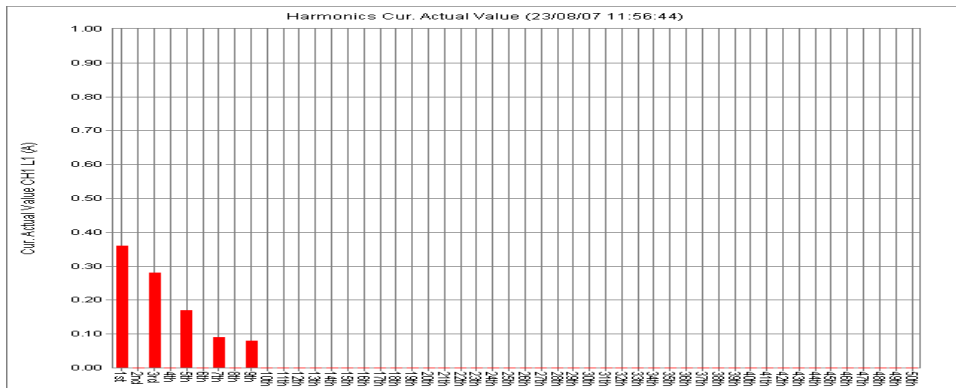


Figure 2.13 Current harmonic spectrums (fan regulator)

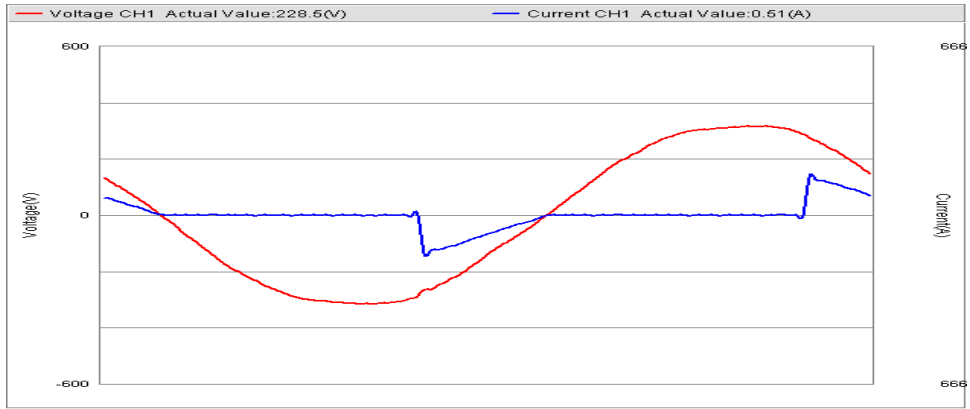


Figure 2.14 Voltage and current waveform (fan regulator)

2.2.2.2 Personal computer (PC)

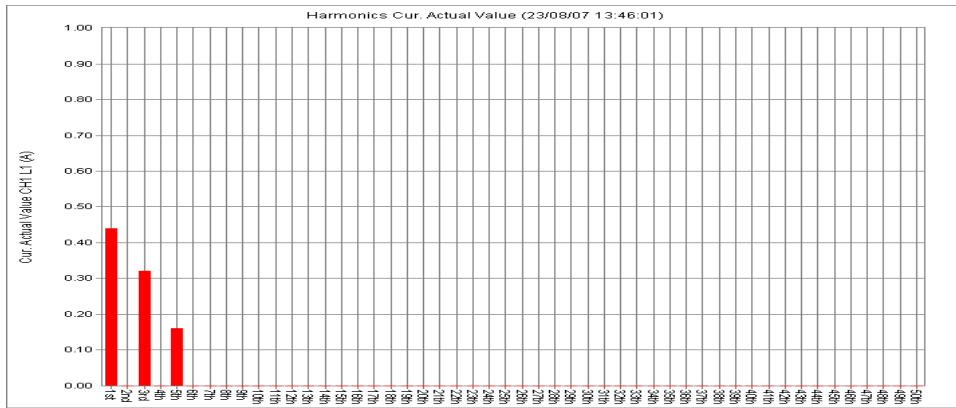


Figure 2.15 Current harmonic spectrum (PC)

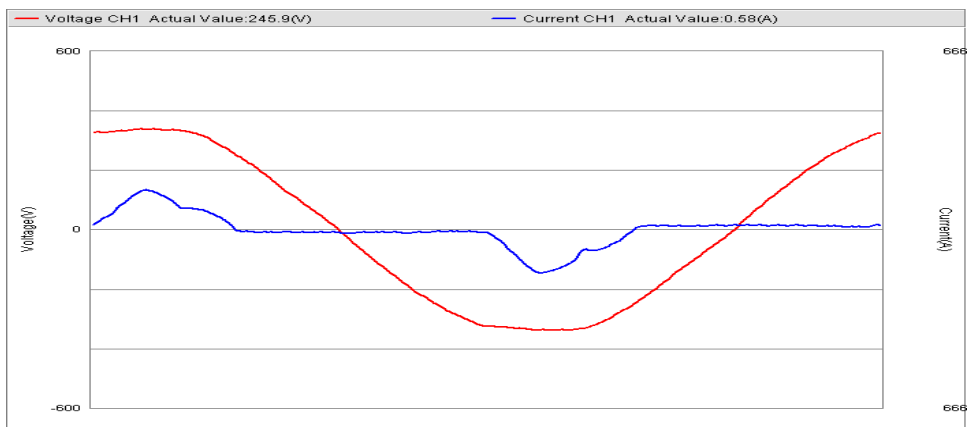


Figure 2.16 Voltage and current waveform (PC)

2.2.2.3 Printer

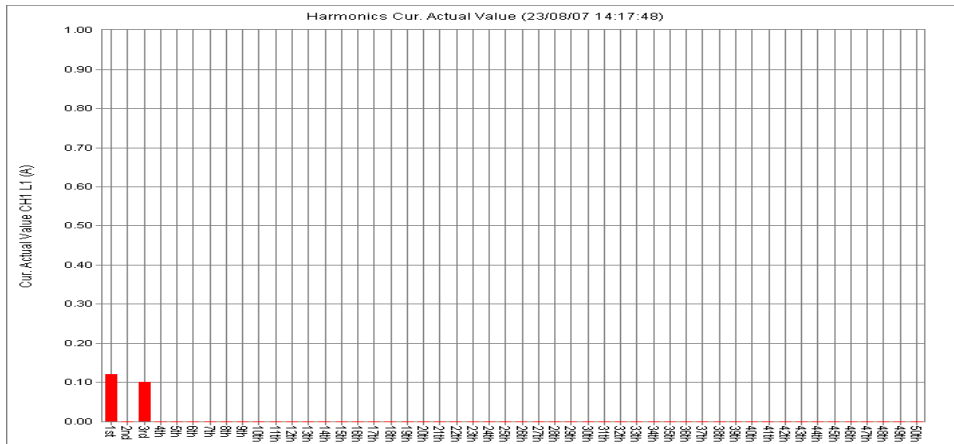


Figure 2.17 Current harmonic spectrums (Printer)

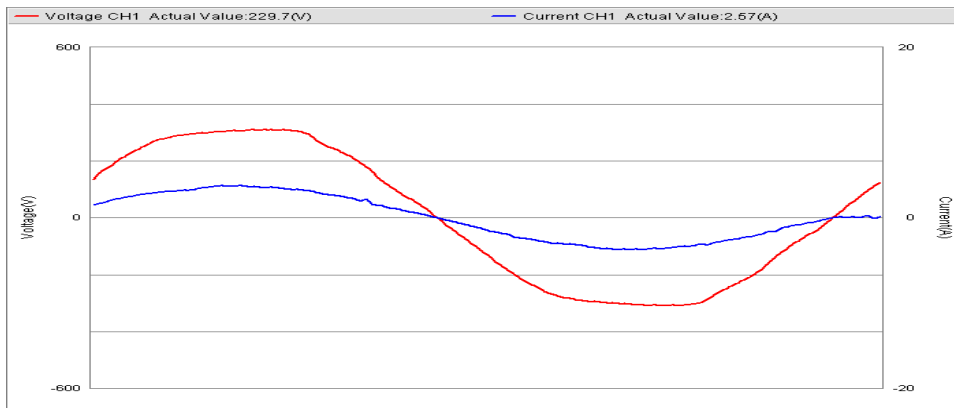


Figure 2.18 Voltage and current waveform (Printer)

2.2.2.4 LCD projector

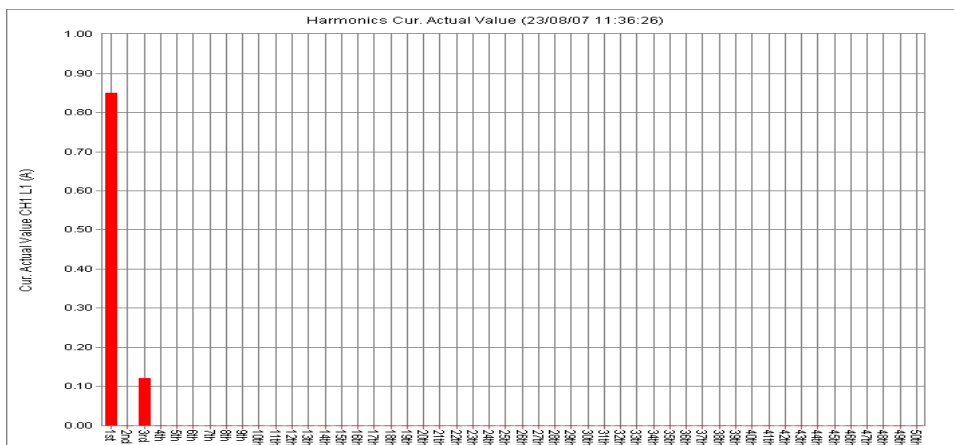


Figure 2.19 Current harmonic spectrums (LCD projector)



Figure 2.20 Voltage and current waveform (LCD projector)

2.2.2.5 Cathode ray oscilloscope (CRO)

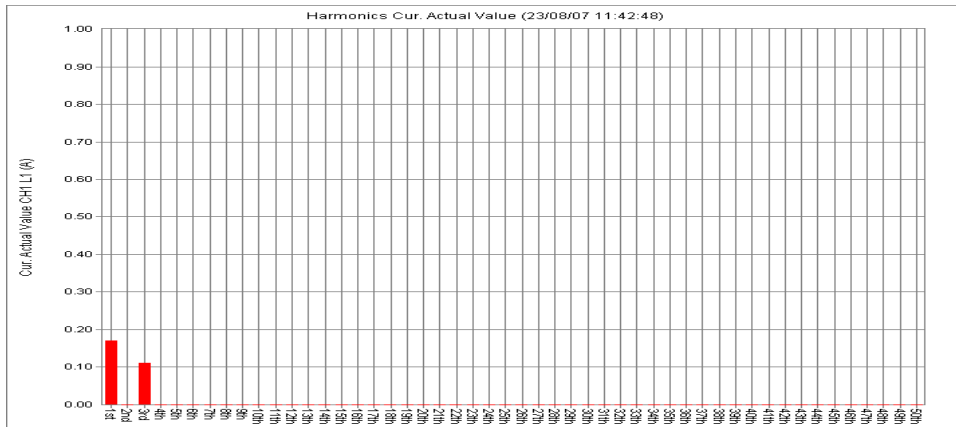


Figure 2.21 Current harmonic spectrums (CRO)

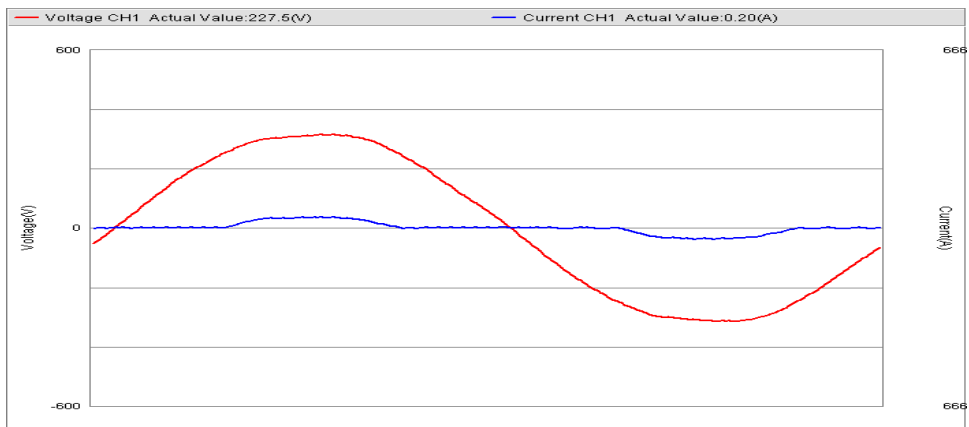


Figure 2.22 Voltage and current waveform (CRO)

2.2.2.6 Distribution transformer secondary (DT)

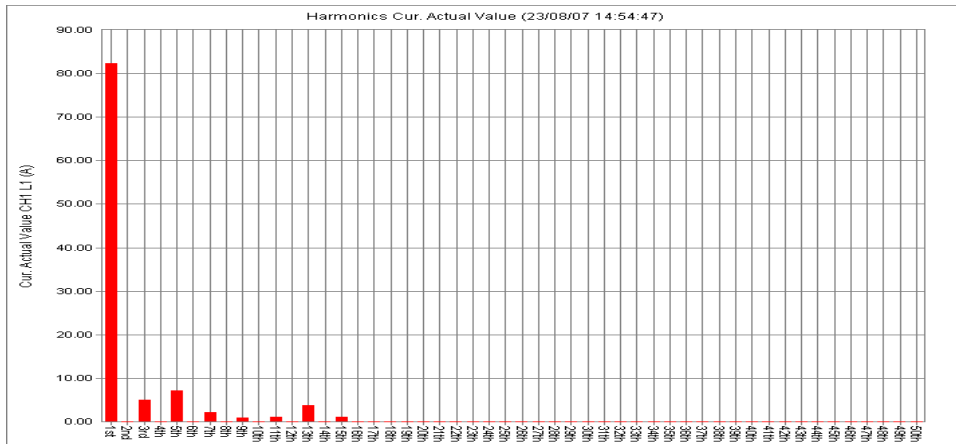


Figure 2.23 Current harmonic spectrums (DT)

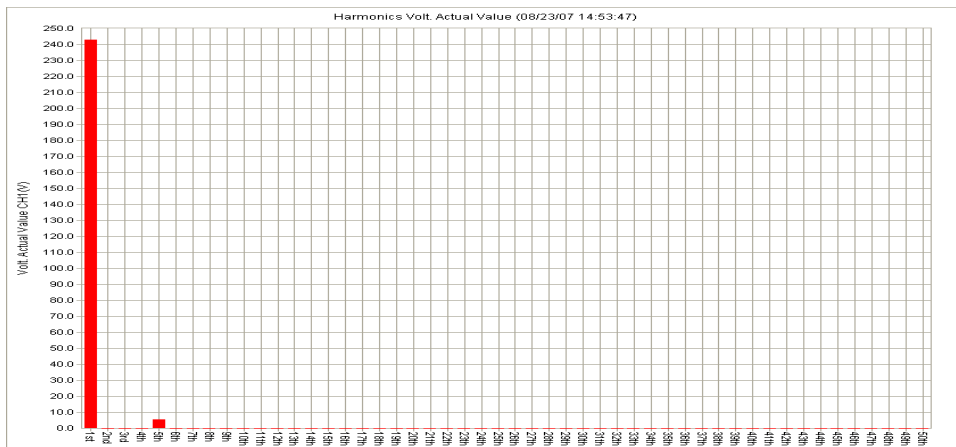


Figure 2.24 Voltage harmonic spectrums (DT)

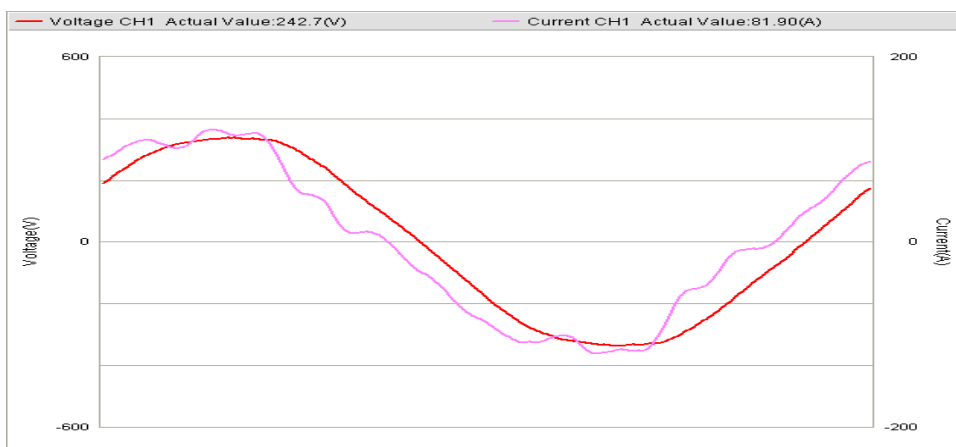


Figure 2.25 Voltage and current waveform (a-phase)

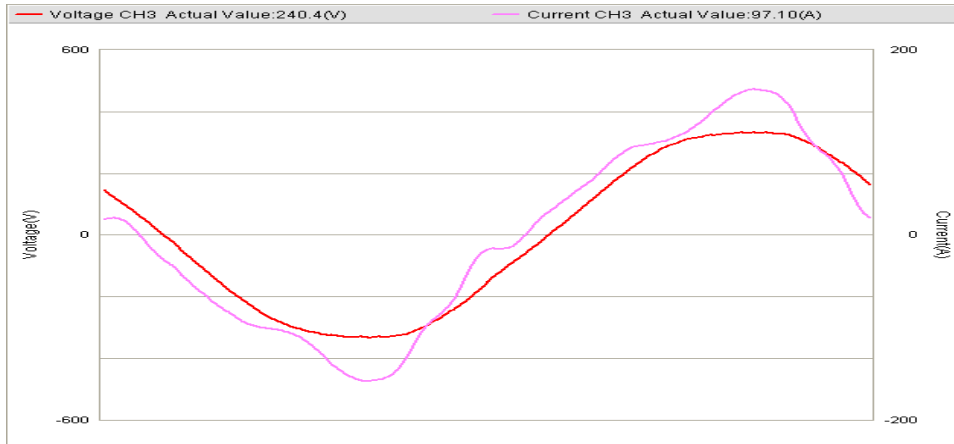
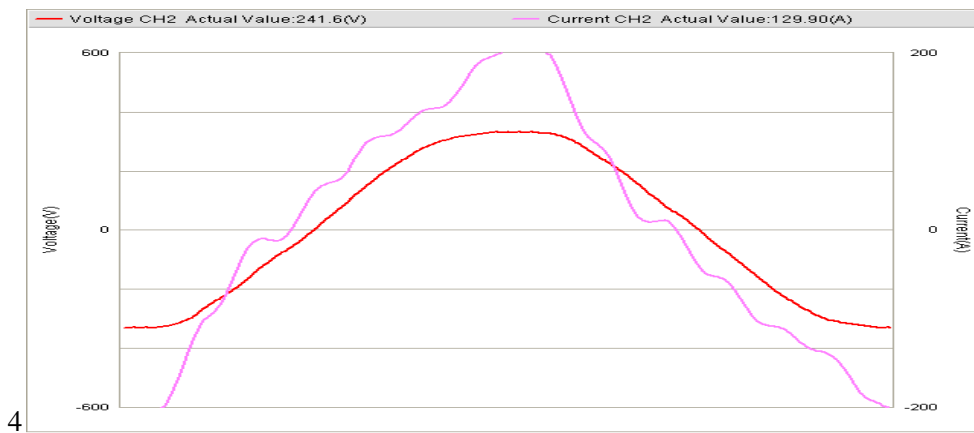


Figure 2.26 Voltage and current waveform (b-phase)



4

Figure 2.27 Voltage and current waveform (c-phase)

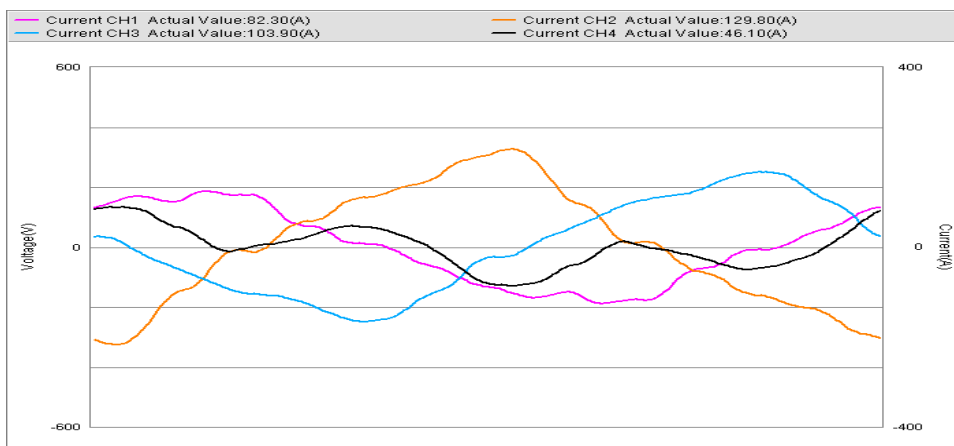


Figure 2.28 Voltage and current waveform (a-b-c and neutral)

Total harmonic distortions of domestic and industrial loads are summarized in Table 2.1.

Table 2.1 Total voltage and current harmonic distortion

Industrial non-linear loads			
Sr. No.	Non-linear load	THD_V %	THD_I %
1	Laser Machine	2.4	36.19
2	Embroidery Machine	0	17.4
3	Water Jet (Textile Industries)	0.5	9.3
4	Arc Furnace	2.5	86
5	UPS	2.4	50.83
Domestic non-linear loads			
6	Computer Centre	2.1	16.9
7	Electronic Fan Regulator	2.24	96.94
8	Personal Computer	2.1	83.33
9	Printer	4.33	22
10	LCD Projector	2.1	14.11
11	CRO	2.1	64.7
12	Distribution Transformer	2.2	12

As shown in Table 2.1 THD_V for industrial loads is ranging from 0 % to 2.5 %, whereas for domestic loads is 2.1 to 4.33 %. Similarly, THD_I for industrial loads and domestic loads is ranging from 9.3 % to 50.83 % and 12 % to 96.94 % respectively. As discussed in the previous chapter, the limit imposed for maximum harmonic distortion by IEEE-519, 1992 is 5 % for both THD_V and THD_I . It can be seen that the industrial and domestic loads are satisfying IEEE limits for THD_V but exceeding limits for THD_I . Electric arc furnace is chosen as typical industrial non-linear load for simulating distribution network.

2.3 Electric Arc Furnace

The increasing iron demand, such as in vehicle industries, encourage the steel-works to invest more and more in the recovery of metals. The EAF is used to provide high quality steels from a raw material of steel scrap.

2.3.1 Typical EAF

Typical EAF is shown in Fig. 2.29. It consists of a refractory lined shell and removable roof.

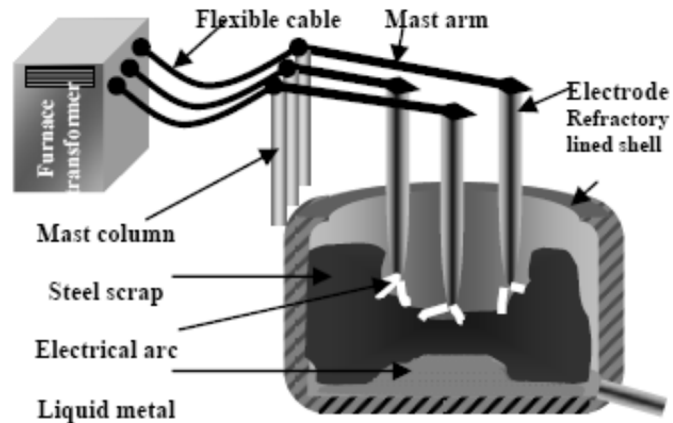


Figure 2.29 Typical electric arc furnaces (EAF)

Three graphite electrodes, held in clamps on the end of a supporting mast arm, pass through holes in the furnace roof. Electrical power is supplied to the electrodes by an adjustable voltage tap transformer, and the heat generated by electric arcs striking between the electrodes and the scrap melts the steel, as shown in Fig. 2.30.

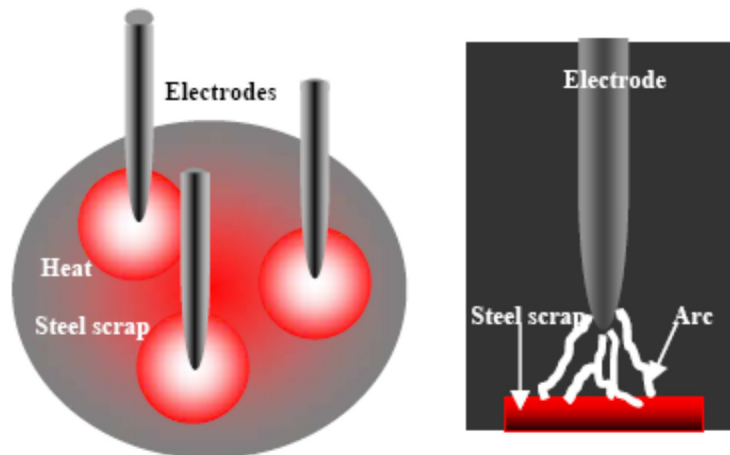


Figure 2.30 Heat conversions by electric arc

The maximum electrical power to heat conversion occurs for a particular length of arc [72], and any deviation from this optimum length diminishes the power utilization efficiency. The steel scrap surface is irregular by nature of the scrap, and, as parts of the scrap melt, it moves about, changing the contours of the surface. Thus, random disturbances in the arc length occur continuously. It is the function of the position control system to respond to such disturbances by moving the electrode to maintain the arc length at its pre-set value [73].

2.3.2 Typical EAF Process

In EAF scrap is melted by means of an electric arc. The normal operation stage of EAF is divided into two parts [1]:

- The meltdown stage: It requires a stable arc, and hence operators normally lower the electrode to keep the stable arc in the system.
- The refining stage: A long arc is required in this case.

The operation of EAF is mainly governed by [1],

- The operation stage
- The electrode control strategy
- The system parameters

First of all the furnace is charged with scrap, after that the electrodes could be lowered, each of which has its own regulator and mechanical drive. The electrodes are connected to the furnace transformer, which may be rated from 90 to 265 volts. To achieve meltdown as quickly as possible one must follow the following stages [58],[74]:

1. The current is initiated by lowering the electrodes, above the material.
2. Electrodes bore through the scrap to form a pool of liquid metal.
3. Electrical arc will be lengthened by increasing the voltage to maximum power.
4. Arc length is changed so that the shorter arc will deliver a higher portion of its heat to the metal below the electrode.
5. Chemical treatments to improve steel quality are done under low power to maintain steel liquid.
6. Stop melting.

2.3.3 Typical EAF PQ issues

The increasing popularity of EAF in metallurgical industries to melt scrap causes significant impacts on power system. EAF is responsible for deteriorating the power quality in the network by,

- Introducing harmonics
- Propagating voltage flicker
- Propagating transient voltage

EAFs are time-variant and non-linear loads. EAF creates following PQ problems [75]:

- Odd and even Harmonics
- Voltage flickers
- Unbalanced voltages and currents

2.4 EAF Modeling

The EAF load is non-linear, time-variant in nature by inherence which results in to power quality problems such as-current and voltage harmonics along with voltage flickers. The EAF operation generates odd and even current harmonics. These current harmonics interact with the system impedance and generate voltage harmonics when circulated in the electric network. These current and voltage harmonics together can affect other consumers connected in the distribution network. The EAF is also an inherent large source of voltage flicker. The voltage flicker is defined as the sensation that is experienced by human eye when subjected to changes in the illumination intensity in the frequency range of 5 to 15 Hz [76]-[77]. The voltage flicker can causes large voltage fluctuation in the connected distribution which in turn affects operation of other connected loads in the distribution network. Therefore, EAF modeling has attracted power system engineers to solve these power quality issues.

2.4.1 Arc Modeling

Simulation of arc is an important issue in EAF modeling. Several methods describing the electric arc are available in the literature [59], [78]-[79] and [81]-[83]. On the basis of actual measured samples of an electric arc in several functioning cycles of EAF, different operating points are generated in the form of statistical probability, corresponding to hidden Markov theory in [80]. This requires actual measurement of an electric arc. The time domain model

utilizing differential equations are presented in [59]. Variation of power transmitted to the load by the arc furnace during the cycle of operation is considered in [81]. Balanced steady state equations are used in [82]. Comparison of the time domain and frequency domain EAF models emphasizes use of time domain models [78], [83]. Frequency response and VIC are taken in to account to analyze the EAF behavior in [83]. These methods impose limitations such as prior knowledge of initial conditions in case of the differential equations, consideration of balanced three phase currents, use of complicated mathematics and actual arc measurement for the EAF modeling. A new time domain approach is proposed in EAF modeling which is validated by simulation and comparing its various performance characteristics with existing Cassie-Mayr's EAF model in MATLAB environment that of available real measured data. The main features of the proposed EAF model are good mathematical approximation, no need of initial conditions, and no need of measurements in actual arc and consideration of unbalanced three phase currents. The proposed model can be used to describe various operating cycles of electric arc furnace and its impact on the connected electric network from power quality point of view. Finally, the proposed method presents a suitable model with a very good approximation for the VIC. In order to increase the accuracy of the load model, a random noise is employed to establish a new model of the furnace load.

2.4.2 Cassie-Mayr's EAF Model

Classical arc models are based on the energy conservation principle describing the arc as an electro-thermal system with an internal source term due to Joule heating and exchanging heat with the surrounding, colder environment. If Joule heating is higher (lower) than energy dissipation to the outer environment, then the arc energetic content increases (decreases). Since the arc electric conductivity is related to the arc energetic content, the electric characterization of the arc as a component of a network is thus produced.

In 1939 Cassie proposed a model of arc in which the arc was assumed to have cylindrical column with uniform temperature and current density, so that its area varies to accommodate the change in current. The power dissipation was assumed to be proportional to the column cross section [84]-[85]. The electric current is relatively high (>500A) and the model is thus unsuited for describing arcs in the vicinity of current zero. A few years later, in 1943, Mayr

proposed a somewhat improved model, in which arc was assumed to be of fixed diameter but of varying temperature and conductivity, the power loss occurred from the surface of the arc only [86]-[87]. Mayr assumed power losses are caused by thermal conduction at small currents. This means that the conductance is strongly temperature dependent but fairly independent of the cross-section area of the arc. The area is therefore assumed constant. The electric current is relatively low (say 500A) and the model is thus suited for describing arcs in the vicinity of current zero, at least not too close to the current zero. This model is applicable for analyze of residual current, which is arisen after current interruption. This stadium is called as a thermal regime and its time interval of persistency is units of 10-6seconds [88]-[89].

It has been found that Cassie's model best describes the period before current zero where as Mayr's model represent better the post arc regime. Thus Cassie's theory was looking at high current arcs with convection as the dominant energy transfer feature while Mayr's paper was looking at low current arcs with thermal conduction transfer as the main feature for current zero behavior.

Mathematical model of Cassie-Mayr EAF model expressed as in [59], [81]:

$$g = g_{\min} + \left[1 - \exp\left(-\frac{i^2}{I_0}\right) \right] \cdot \frac{v \cdot i}{E_0^2} + \exp\left(-\frac{i^2}{I_0}\right) \cdot \frac{i^2}{P_0} - \theta \cdot \frac{dg}{dt} \quad (2.3)$$

$$\theta = \theta_0 + \theta_1 \cdot \exp(-\alpha \cdot |i|) \quad (2.4)$$

$$v = \frac{i}{g} \quad (2.5)$$

Typical values of and $E_0, \theta_0, \theta_1, \alpha, P_0, I_0,$ and g_{\min} and are tabulated in Table 2.2. The required data was taken from [59], [81] for reference. Combined Cassie-Mayr arc model provide a qualitative description of the arc phenomena in the low and high current regions respectively.

Table 2.2 Parameters of Cassie-Mayr's EAF Model

Parameters	Value
g_{\min}	0.008
I_0 (kA)	20
E_0 (V)	250
P_0 (kW)	100
θ_0	110e-06
θ_1	100e-06
α	0.0005

These models include a differential equation that depends on a set of parameters which should be obtained from experimental data. By selecting a suitable set of arc parameters it is possible to obtain a better approximation to the arc dynamics described by experimental data. However, increasing the number of parameters can lead to difficulties for calculating their magnitudes. In the original formulation of the Cassie model, the hypothesis is that the cooling power be entirely due to convection.

2.4.3 Proposed EAF Model

Typical VIC of an EAF is found to be exponential and hyperbolic in nature [80]. Complete VIC can be obtained by combining hyperbolic and exponential nature of the characteristics. Efforts are already made to combine these characteristics in [77],[82]. These characteristics can also be combined using transition function suggested in [59], [90]. In this paper the same transition function is used to propose a novel EAF model combining the exponential and hyperbolic model characteristics. A brief detail of exponential and hyperbolic model along with the proposed model is as follows:

2.4.3.1 Model 1: Hyperbolic Model

V-I characteristic of hyperbolic EAF model is considered in form of $v = v(i)$ and is described as [77], [82]:

$$v_{hyp}(i) = V_{at} + \left(\frac{C}{D + i} \right) \quad (2.6)$$

V_{at} is the voltage threshold magnitude to which the voltage approaches as EAF current increases. This voltage is dependent on the arc length. These constants can take different values which depend on the sign of the derivative of the arc current and can be obtained in steady state. Table 2.3 shows typical values of various parameters of EAF models.

Table 2.3 Proposed EAF parameters

Parameters	Value
V_{at0} (V)	200
C (kW)	19
D (kA)	5
I_0 (kA)	20
I_r (kA)	20

2.4.3.2 Model 2: Exponential Model

V-I characteristic of exponential EAF model is described as [79], [82]:

$$v_{exp}(i) = V_{at} \left(1 - e^{\left(\frac{i}{I_0} \right)} \right) \quad (2.7)$$

In equation (2.7) I_0 is a current constant employed to model the steepness in positive and negative phases of arc currents. A typical value of I_0 is tabulated in Table 2.3.

2.4.3.3 Model 3: Proposed Model

Exponential and hyperbolic models can be combined into single model by defining a transition function $O(i)$, which is a function of arc current and is given by:

$$v_{com}(i) = \underbrace{[1 - O(i)]}_{\text{Higher Current}} \cdot v_{exp} + \underbrace{O(i)}_{\text{Lower Current}} \cdot v_{hyp} \quad (2.8)$$

In equation (2.8) v_{hyp} and v_{exp} are the arc voltages given by equations (2.6) and (2.7) respectively. A satisfactory form of $O(i)$ used in this combination is given in [59], [81]:

$$O(i) = e^{\left(\frac{i^2}{I_t^2}\right)} \quad (2.9)$$

In equation (2.9) I_t is the maximum value of arc current variation. When arc current (i) is small, value of $O(i)$ is approaching unity which yields arc voltage value v_{com} is dominated by v_{hyp} and when arc current value is large, $O(i)$ is approaching zero yields arc voltage value v_{com} is dominated by v_{exp} . The exponential and hyperbolic functions are mathematically joined to make arc voltage to follow exponential model characteristic during high arc currents and to follow hyperbolic model characteristic during low arc currents.

Finally the V-I characteristic of the proposed model is described by following combined equation:

$$v_{com}(i) = \begin{cases} V_{at} \left[1 - e^{\left(\frac{i}{I_o}\right)} \right] & \text{for higher arc current} \\ V_{at} + \left(\frac{C}{D+i} \right) & \text{for lower arc current} \end{cases} \quad (2.10)$$

It can be seen from equation (2.10), for the positive current and regarding the hysteresis property of the arc, there are two cases. To increase and decrease the current of the EAF, the hyperbolic equation and exponential-hyperbolic form of the equation are used, respectively. The proposed method can describe EAF behavior in time domain using differential equation [90]. In addition, it is able to analyze the behaviors in the frequency domain without solving the sophisticated differential equations. Moreover, the proposed EAF model can describe various operating conditions such as scrap meltdown stage, refining stage from power quality point of view. The results agree with actual conditions of the EAF in the steel industries.

2.4.4 EAF Simulation with Power System

Fig. 2.31 shows a single phase equivalent circuit of an EAF supplied by source.

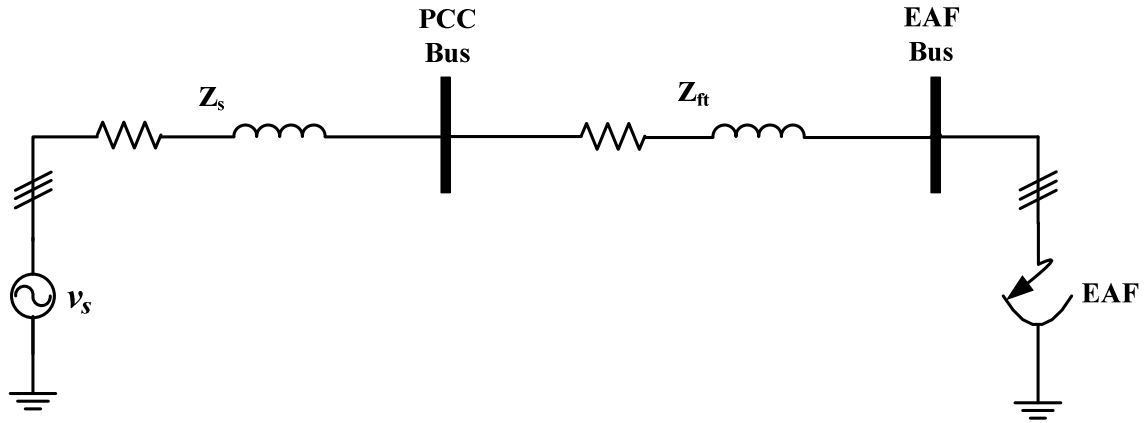


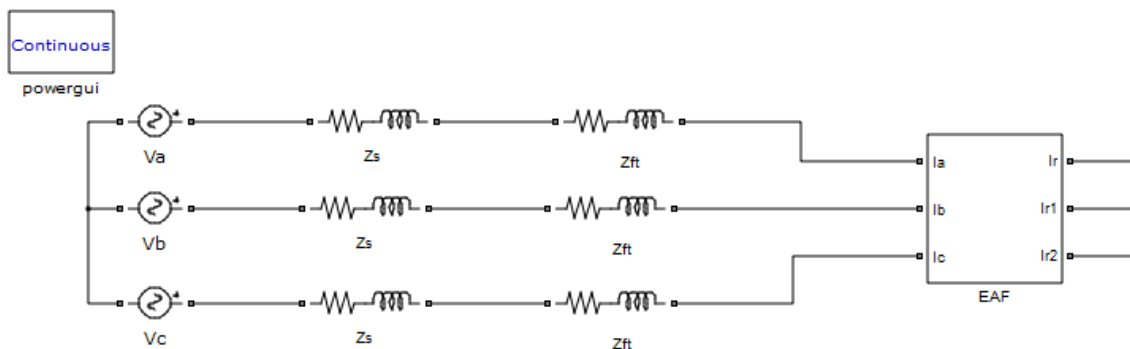
Figure 2.31 EAF with an electric network

Table 2.4 shows power system parameters along with proposed EAF Model. The power system data for simulation was taken from [81], [83].

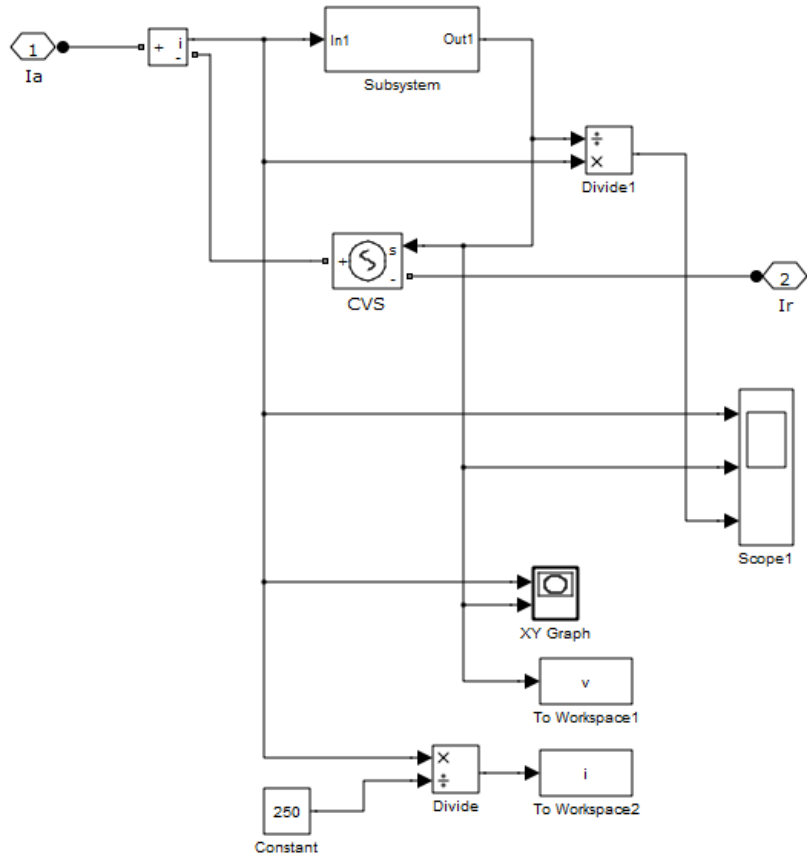
Table 2.4 EAF Power system parameters

Parameters	Value
V (V)	240
f (Hz)	50
Z_s (m Ω)	(0.0527+j0.467)
Z_{ft} (m Ω)	(0.3367+j3.23)

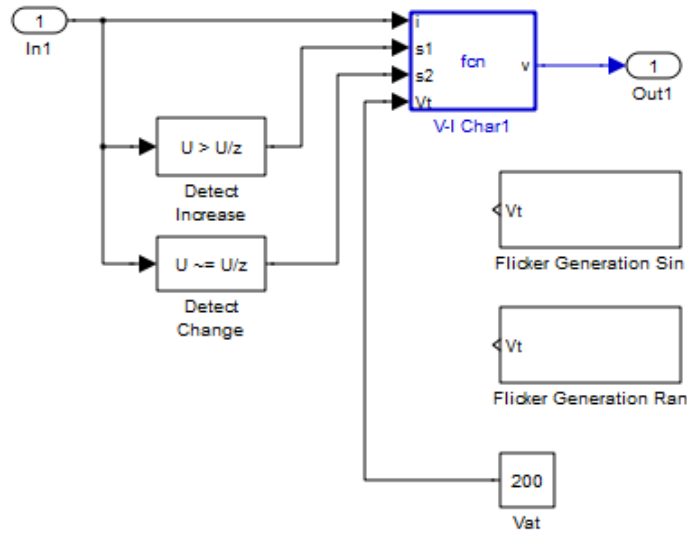
Figure 2.32 shows complete simulation of three-phase electric network supplying an EAF using Simulink/MATLAB platform.



(a)



(b)



(c)

Figure 2.32 Complete Simulink/MATLAB Simulation file of the proposed EAF model (a) three phase network along with EAF (b) single phase EAF simulation (c) EAF equation modeling

As shown in Fig. 2.32 (a), three phase power source is simulated by considering three single phase voltage source (v_a , v_b and v_c) shifted by 120 electrical degrees each. System impedance and furnace transformer impedance is represented by three elements for three phases. A non-linear time varying voltage controlled source is used as function to represent EAF model as shown in Fig. 2.32 (b). The arc current acts as an input to this function which results in to non-linear time varying voltage as an output. Such three elements are connected in star to form three phase EAF model. Fig. 2.32 (c) shows simulation of the proposed EAF model equation (see Appendix A). Three phase voltage, current measurements along with active power, reactive power and factor measurements are done at PCC.

2.5 Performance Characteristics Comparison

Performance of EAF includes various performance characteristics such as arc current, arc voltage, harmonic spectrum, arc conductance variation, arc VIC, variation in active & reactive power, etc. Comparisons of performance characteristics of the proposed EAF model with that of existing Cassie-Mayr's EAF model and real measured available data are presented in this section. For better comparison, each performance characteristic of the proposed EAF model and the Cassie-Mayr's model.

2.5.1 Steady State Characteristics (Refining cycle)

Steady state characteristic of EAF is exhibited mainly during refining cycle. The level of molted material is constant along with uniform rate of melting in the furnace. Arc length is almost constant during this cycle resulting into uniform VIC. This produces voltage and current harmonics mainly at PCC as shown in Fig. 2.33 to 2.37.

2.5.1.1 Arc voltage and arc current

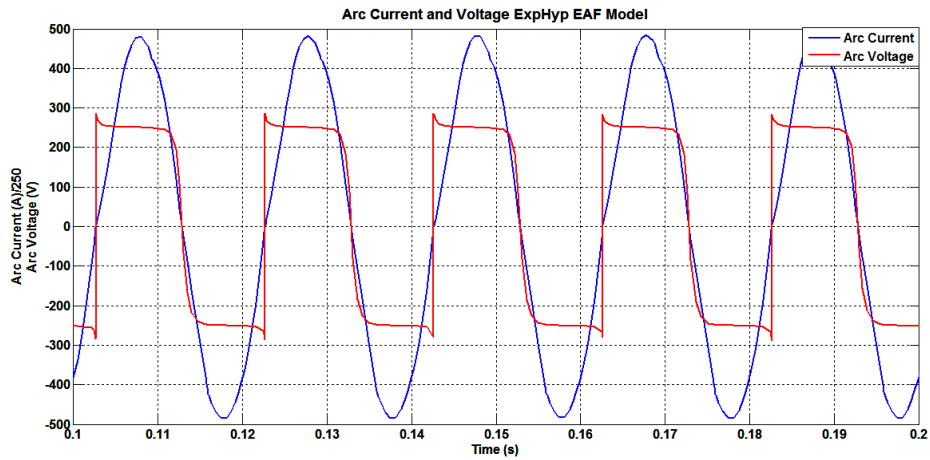
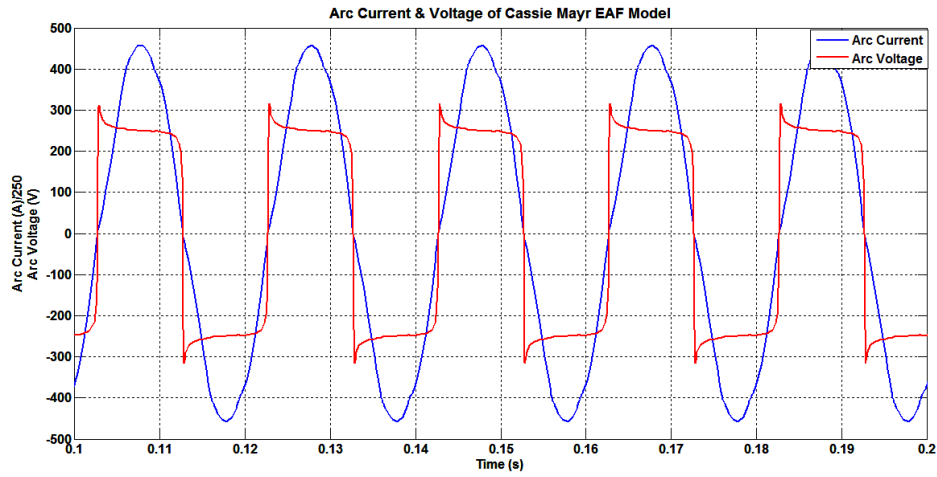
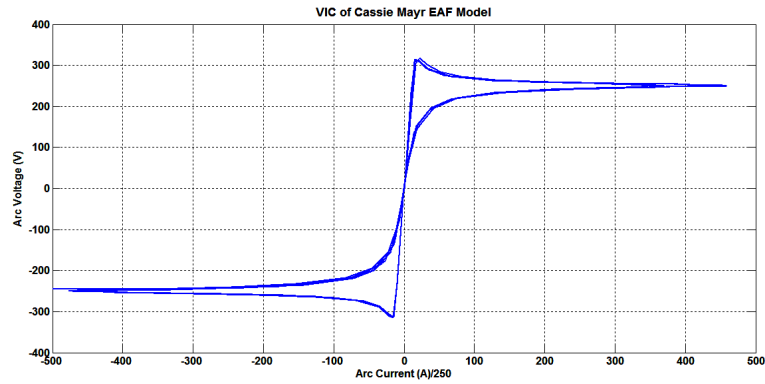


Figure 2.33 Waveform of arc voltage-current v/s time of (a) Cassie-Mayr’s EAF model (b) Proposed EAF model during refining cycle

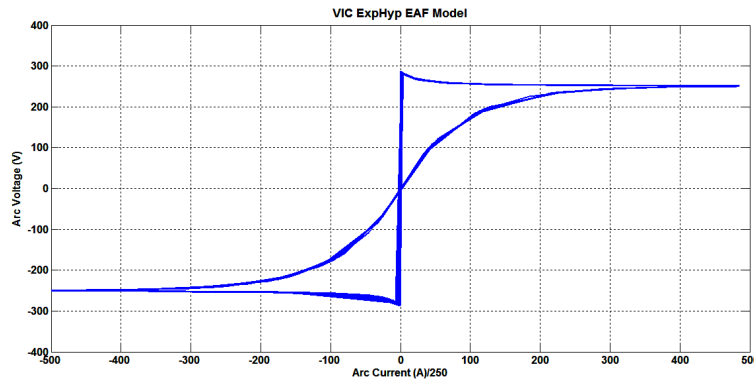
Figure 2.33(a)-(b) shows waveform of arc voltage and arc current at PCC generated by Cassie-Mayr’s EAF model and the proposed EAF model respectively. It can be noted that the magnitude and the shape of both-the voltage and the current waveform-are identical, which confirms validity of the proposed model. Simulated results of arc voltage and arc current are typically same as real EAF waveforms [91]-[95].

2.5.1.2 VIC

Figure 2.34 (a)-(b) shows VIC produced by Cassie-Mayr's EAF model and the proposed EAF model respectively, which are identical in shape and in values. The comparison between the VIC obtained by the proposed EAF model with that of acquired by real measured data shows that the VICs are identical in nature [93]-[95], which confirms validity of the proposed EAF model on practical ground.



(a)

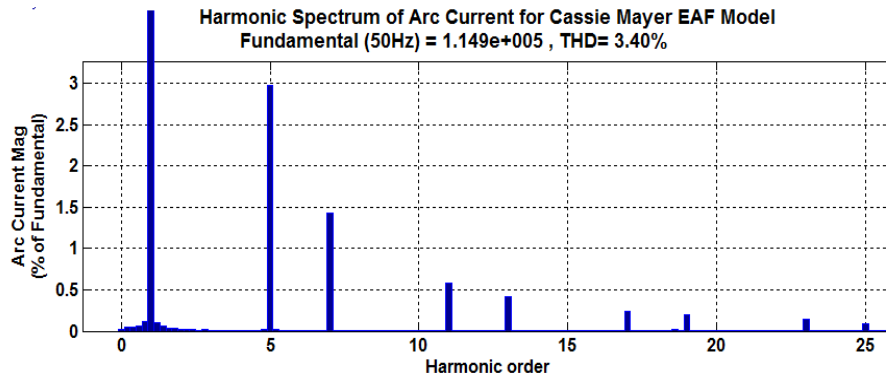


(b)

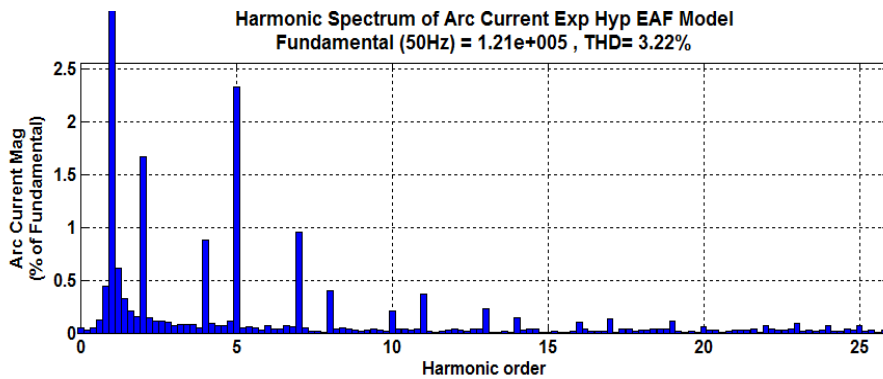
Figure 2.34 VIC of (a) Cassie-Mayr's EAF model (b) the proposed EAF model during refining cycle

2.5.1.3 Current harmonics

Figure 2.35 (a) and Figure 2.35 (b) represents harmonic spectrum of arc current of the Cassie-Mayr's EAF model and the proposed EAF model respectively.



(a)



(b)

Figure 2.35 Harmonic spectrum of arc current at PCC of (a) Cassie-Mayr’s EAF model (b) the proposed EAF during refining cycle

It can be noted from Figure 2.35 THD observed in the arc current of both the models is nearly equal (3.40 % for Cassie-Mayr’s EAF model and 3.22 % for the proposed EAF model). This shows validity of the proposed EAF model for refining cycle. % Harmonic distortions of individual harmonic orders (5th, 7th, 11th, 13th, 17th, 19th, 23rd and 25th) are tabulated in Table 2.5. Table 2.5 shows comparison of current harmonic analysis among the Cassie-Mayr’s EAF model, the proposed EAF Model, and real measured data [94]. Also odd harmonics of very low magnitude are observed as EAF generates odd harmonics.

% Error observed in THD of the proposed EAF model with respect to the Cassie-Mayr’s EAF model is 5.29 %, which is less than 10 %. It makes the proposed EAF model acceptable.

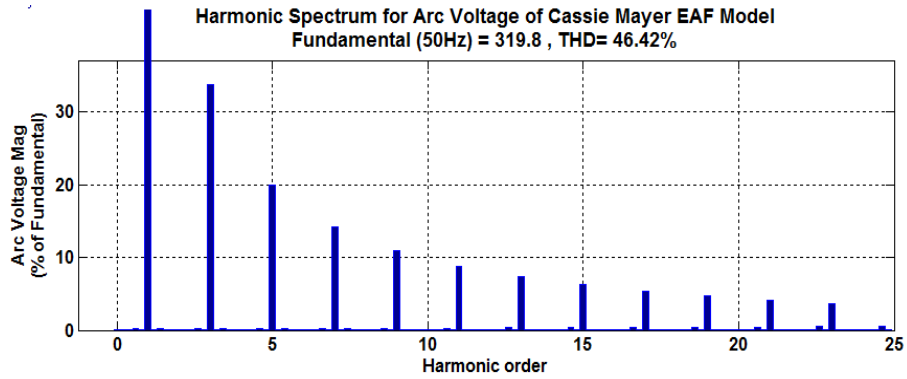
Table 2.5 Current harmonic analysis

Harmonics (%)	Cassie-Mayr's EAF model	Proposed EAF model	Real measured data	% Error in (w. r. t. Cassie-Mayr)	% Error (average) w. r. t. Cassie-Mayr	% Error in (w. r. t. real measured data)	% Error (average) w. r. t. real measured data
I_{peak} (A)	117.5	120	127.05	-2.13	+7.05	5.55	-3.21
THD_I	3.4	3.22	2.98	5.29		-8.05	
5 th	2.98	2.79	2.56	6.38		-8.98	
7 th	1.43	1.24	1.33	13.29		6.77	
11 th	0.58	0.56	0.52	3.45		-7.69	
13 th	0.42	0.39	0.38	7.14	+7.05	-2.63	-3.21
17 th	0.24	0.22	0.22	8.33		0.00	
19 th	0.19	0.17	0.18	10.53		5.56	
23 rd	0.14	0.13	0.12	7.14		-8.33	
25 th	0.09	0.08	0.07	11.11		-14.29	

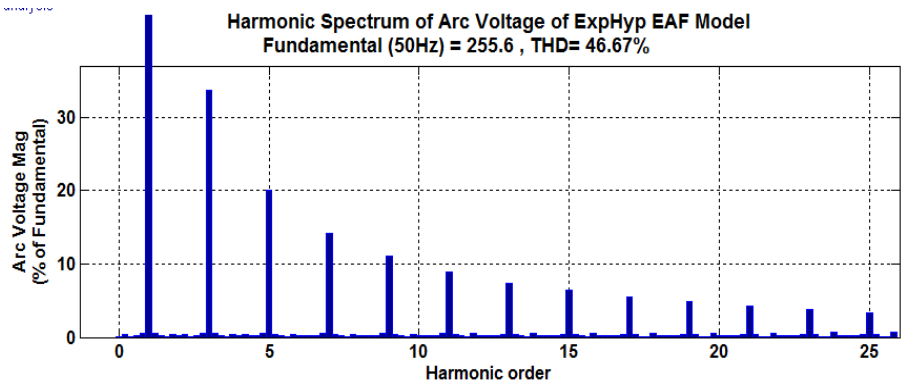
Harmonic distortion of each harmonic order is expressed as % of fundamental as shown in Table 2.5. The proposed EAF model produces individual current harmonic components those are very close in magnitude to the real measured data available [93]. % Error for each harmonic order is calculated by taking the Cassie-Mayr to be the reference. An average error observed is +7.05 % (w. r. t. Cassie-Mayr EAF model) which is less than 10 %. This fact again validates the proposed EAF model. Similarly, w. r. t. real measured data, the average error observed is -3.221% which is also less than 10 %, which again validates the proposed EAF model. % Error observed in the arc current magnitude of the proposed EAF model with respect to the Cassie-Mayr's EAF model is -2.13 %, which again confirms validity of the proposed EAF model.

2.5.1.4 Voltage harmonics

Figure 2.36 (a) and Figure 2.36 (b) represents harmonic spectrum of arc voltage of the Cassie-Mayr's EAF model and the proposed EAF model respectively



(a)



(b)

Figure 2.36 Harmonic spectrum of arc voltage at PCC of (a) Cassie-Mayr’s EAF model (b) proposed EAF model during refining cycle

It can be also noted from Figure 2.36 that the THD observed in the arc voltage of both the models is quite same (46.42 % for the Cassie-Mayr’s EAF model and 46.67 % for the proposed EAF model). This again confirms validity of the proposed EAF model refining cycle. Voltage waveform is distorted due to superimposition of 3rd, 5th, 7th, 9th, 11th, 13th, 15th, 17th, 19th, 21st, 23rd and 25th order harmonics predominantly on fundamental wave. % harmonic distortions of individual harmonic are tabulated in Table 2.6. Table 2.6 shows comparison of voltage harmonic analysis among Cassie-Mayr’s EAF model, the proposed EAF model and real measured data [93]. THD observed in the Cassie-Mayr’s EAF model and the proposed EAF model is 46.42 % and 46.67 % respectively, which is violating IEEE 519-1992 Limits of 5%. % Error observed in THD of the proposed EAF model with respect

to the Cassie-Mayr's EAF model is -0.54 %, which is less than 10 %. It makes the proposed EAF model acceptable.

Table 2.6 Voltage harmonic analysis

Harmonics (%)	Cassie-Mayr's EAF model	Proposed EAF model	Real measured data	% Error in (w. r. t. Cassie-Mayr)	% Error (average) w. r. t. Cassie-Mayr	% Error in (w. r. t. real measured data)	% Error (average) w. r. t. real measured data
V_{peak} (V)	305	288	316	5.57	-1.33	8.86	-1.38
THD_v	46.42	46.67	44.65	-0.54		-4.52	
3 rd	33.69	33.64	32.95	0.15		-2.09	
5 th	19.98	20.07	18.76	-0.45		-6.98	
7 th	14.12	14.19	13.29	-0.49		-6.77	
9 th	10.99	11.05	10.47	-0.54		-5.54	
11 th	8.78	8.92	8.47	-1.57		-5.31	
13 th	7.3	7.41	7.67	-1.48		3.39	
15 th	6.27	6.39	6.46	-1.88		1.08	
17 th	5.36	5.54	5.69	-3.25		2.64	
19 th	4.67	4.82	4.52	-3.11		-6.64	
21 st	4.16	4.29	4.21	-3.03		-1.90	
23 rd	3.65	3.82	3.85	-4.45		0.78	
25 th	3.26	3.38	3.51	-3.55		3.70	

Harmonic distortion of each harmonic order is expressed as % of fundamental as shown in Table 2.6. Harmonic distortion observed in almost all harmonic orders (3rd to 25th) is more than IEEE 519-1992 Limit of 3 % for individual harmonic order. The comparison of each individual harmonic order of the proposed EAF model with that of Cassie-Mayr's EAF model and real measured data confirms validity of the proposed EAF model [93]. Maximum error observed in the proposed EAF model with respect to the Cassie-Mayr's EAF model is +0.15 % (3rd order) and -4.45 % (23rd order) respectively. An average error observed is -

1.33% (w. r. t. Cassie-Mayr EAF model) which is less than 10 %. This fact again validates the proposed EAF model. Similarly, w. r. t. real measured data, the average error observed is -1.38 % which is also less than 10 %, which again validates the proposed EAF model. % Error observed in the arc voltage magnitude of the proposed EAF model with respect to the Cassie-Mayr's EAF model is 5.57 %, which again confirms validity of the proposed EAF model.

2.5.1.5 Active and reactive power (P-Q)

Figure 2.37 shows active and reactive power consumption during refining cycle by the proposed EAF model compared to the existing Cassie-Mayr's EAF model which also agrees with the real measured data [91].

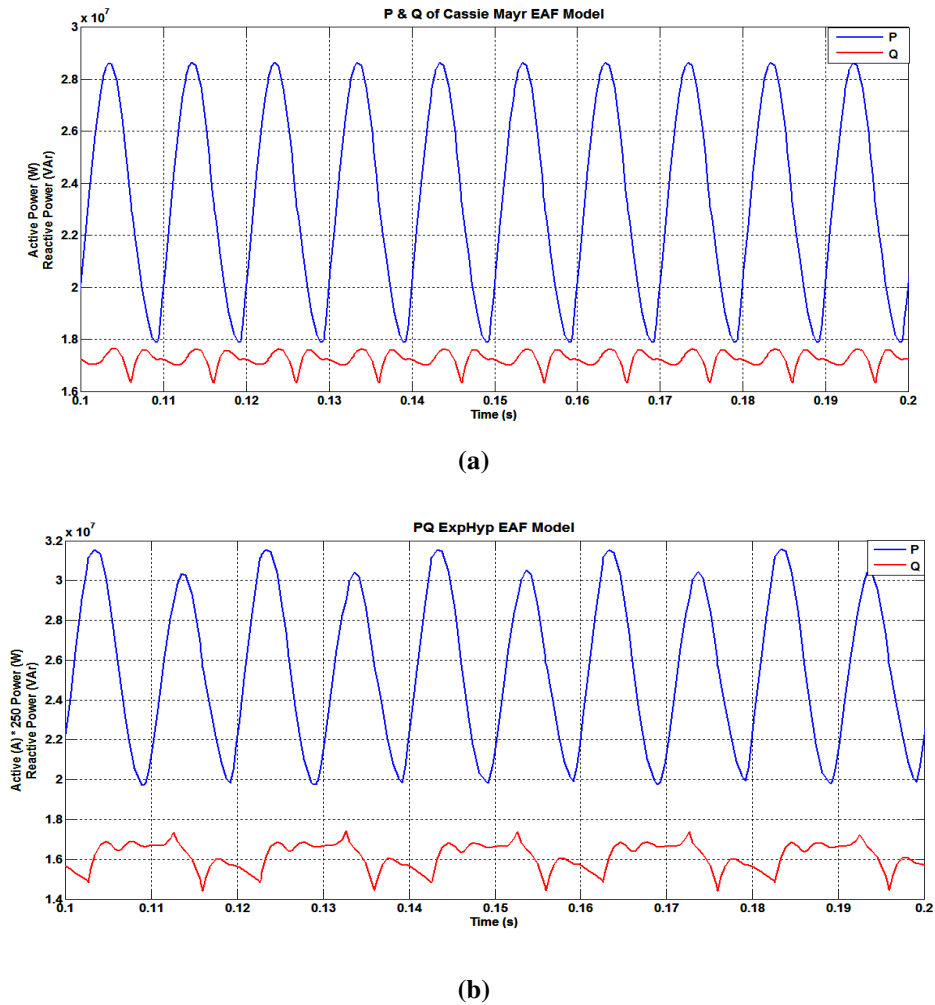


Figure 2.37 P-Q consumption of (a) Cassie-Mayr's EAF model (b) Proposed EAF model during refining cycle

Table 2.7 shows comparison of active power, reactive power and power factor among the Cassie-Mayr's model, the proposed EAF model and real measured data [95].

Table 2.7 Power analysis

Parameter	Cassie-Mayr's EAF model	Proposed EAF model	Real measured data	% Error (w. r. t. Cassie-Mayr)	% Error (w. r. t. real measured data)
P (W)	23280	25900	23497	-11.25	-10.23
Q (VAr)	17250	16130	21357	6.49	24.47
pf	0.574	0.606	0.74	-5.57	18.11

% errors calculated for active power P for the proposed EAF model w. r. t. the Cassie-Mayr's EAF model and that of the real measured data are near than -10%. For reactive power Q and power factor pf , % errors calculated for the proposed model w. r. t. the actual measured data is less than 25 % as shown in Table 2.7, which is little higher.

2.5.2 Dynamic Characteristics (Melting cycle)

Dynamic characteristic represents melting cycle of an EAF. In this operation the furnace is charged with scrap, after that the electrodes could be lowered, each of which has its own regulator and mechanical drive. The steel scrap surface is irregular by nature of the scrap, and, as parts of the scrap melt, it moves about, changing the contours of the surface. Thus, random disturbances in the arc length occur continuously. This operation exhibits severe voltage flickers. Voltage variation with reference to time can be utilized to study voltage flicker effect on the power system with EAF. Effects of sinusoidal and random flicker of the EAF are studied in this section.

Dynamic specifications of EAF at any instant of time are affected by conditions of the furnace at that time and previous instants of the time. The reason for that is when the arc is created, the sudden change in the electrons, ions and gas temperature (that may occur due to sudden change of current) is impossible. Therefore, the sudden change of the current will not lead to sudden change of the arc characteristic. In fact, there is a hysteresis phenomenon in the dynamic of the arc characteristic due to the effects of the current in the previous instants

of time on the present time. The refining stage contributes harmonics in current and voltage, while scrap meltdown stage yields voltage flicker at PCC. Therefore, real time analysis of power quality demands dynamic model of EAF. In order to bring the stationary arc-model to give rise to voltage fluctuations, cause of flicker, the VIC must undergo time variations which correspond to a time dependence of the arc length as [96]-[97]:

$$V_{at} = A + B \cdot l \quad (2.11)$$

A variation in arc length is root cause of typical dynamic behavior of EAF. The arc length can be varied by varying arc voltage directly. In actual practice the variation in arc length is of random in nature. Two types of arc length variations are considered for simulation purpose-sinusoidal and random. Effect of voltage flicker on the power system can be studied by varying V_{at} as follows:

2.5.2.1 Sinusoidal variation

Mathematically the sinusoidal variation can be expressed as [83], [90]:

$$v_{at}(t) = V_{at0} [1 + m \cdot \sin(\omega_f \cdot t)] \quad (2.12)$$

Table 2.8 shows parameters used for sinusoidal variation.

Table 2.8 Parameters for sinusoidal variation

Parameter	Value
V_{at0} (V)	200
m	0.8
ω_f (Hz)	4

Figure 2.38 shows MATLAB simulation of sinusoidal flicker generation.

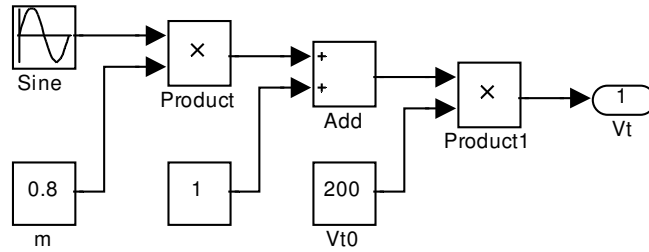


Figure 2.38 Simulink/MATLAB Simulation of sinusoidal flicker generation

Voltage flicker assessment is also one of the important aspects of power quality analysis. The assessment of voltage flicker involves the derivation of system RMS voltage variation and the frequency at which the variation occurs. The voltage flicker usually expressed as the RMS value of the modulating waveform divided by the RMS value of the fundamental value, as follows [98]-[100]:

$$\% \text{ Voltage Flicker} = \frac{\text{RMS Voltage of Modulating waveform}}{\text{Average RMS Voltage}} \quad (2.13)$$

$$\text{RMS Voltage of Modulating waveform} = \frac{\Delta V}{\sqrt{2}} = \frac{V_{2P} + V_{1P}}{2\sqrt{2}} \quad (2.14)$$

$$\text{Average RMS Voltage} = \frac{\left(\frac{V_{2P}}{\sqrt{2}}\right)}{2} - \frac{\left(\frac{V_{1P}}{\sqrt{2}}\right)}{2} = \frac{V_{2P} - V_{1P}}{2\sqrt{2}} \quad (2.15)$$

Substituting equations (2.14) & (2.15) into equation (2.13), we get:

$$\% \text{ Voltage Flicker} = \frac{V_{2P} + V_{1P}}{V_{2P} - V_{1P}} \quad (2.16)$$

Equation (2.16) is useful for voltage flicker estimation.

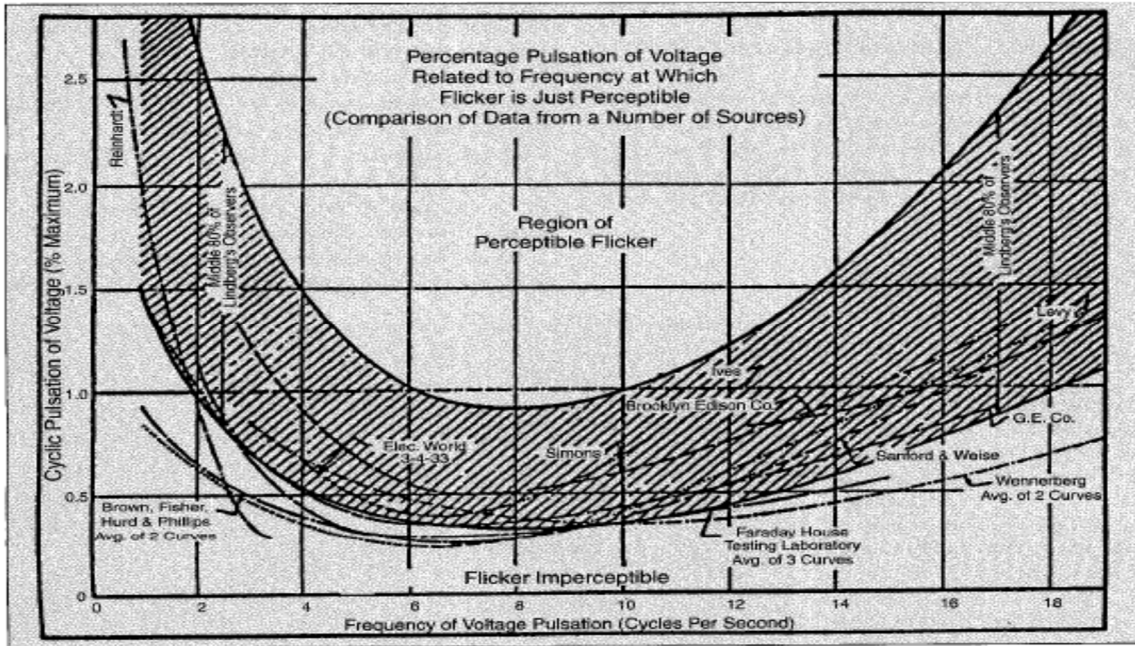
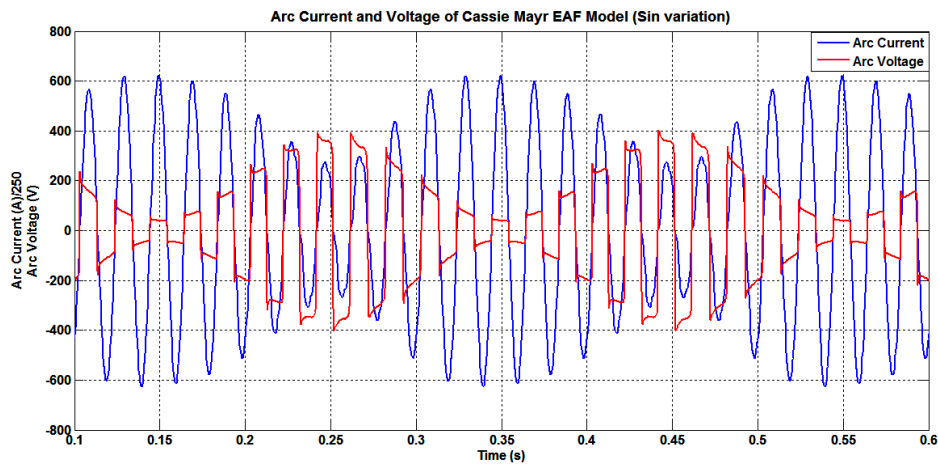


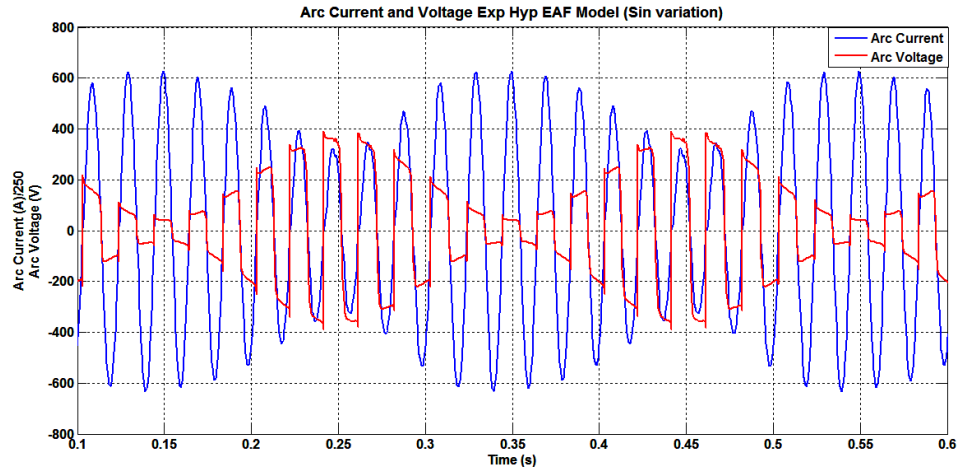
Figure 2.39 Comparisons of data from various sources on voltage flicker

A variety of perceptible/limit curves are available in published literature which can be used as general guidelines to verify whether the amount of flicker is a problem or not [98]-[100]. Comparison of data from various sources for perceptible flicker is given in [98]. Figure 2.39 shows a comparison of data from various sources for perceptible flicker [98]. By frequency of voltage pulsation and % cyclic voltage pulsation, calculated by equation (2.16), it is possible to judge whether voltage flicker is perceptible or not [100].

2.5.2.2 Arc current & arc voltage considering sinusoidal variation



(a)



(b)

Figure 2.40 Waveform of arc voltage-current v/s time of (a) Cassie-Mayr’s EAF model (b) proposed EAF model during melting cycle considering sinusoidal flicker

Figure 2.40 shows simulation results obtained using equations (2.12) along with tabulated parameters given in Table 2.8 for sinusoidal flicker. It indicates variation of arc voltage and arc current with flicker frequency. It can be observed from Figure 2.40(a) and Figure 2.40(b) that the variations observed in arc voltage and arc current in the proposed EAF model and the existing Cassie-Mayr’s EAF model are identical and are also comply with the real measured data available in [91] confirming validity of the proposed EAF model.

Voltage flicker is calculated using equation (2.16) for the Cassie-Mayr’s EAF model and the proposed EAF model and are tabulated in Table 2.9.

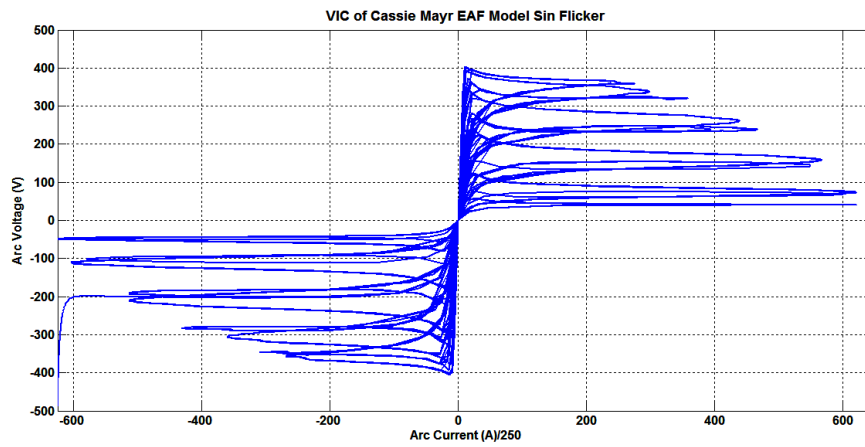
Table 2.9 Voltage flicker analysis

Parameter	Cassie-Mayr’s EAF model	Proposed EAF model	Real measured data	% Error (w. r. t. Cassie-Mayr)	% Error (w. r. t. real measured data)
Voltage measurement					
V_{1P} (V)	65	64		+1.54	
V_{2P} (V)	390	400		-2.56	
% Voltage flicker calculation					
% Voltage flicker	1.39	1.38	+1.40	+0.72	+1.42

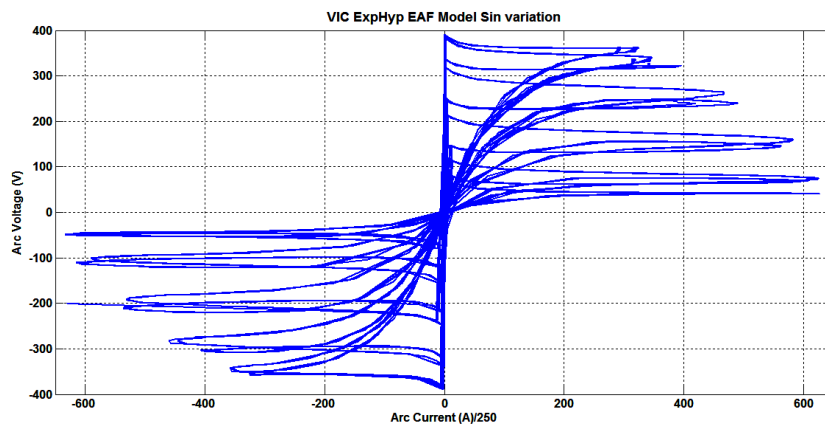
Table 2.9 shows comparison of % voltage flicker generated among the Cassie-Mar's EAF model, the proposed EAF model and real measured data [95]. % errors calculated for the proposed EAF model w. r. t. the Cassie-Mayr's EAF model and that of the real measured data are +0.72 % and +1.42 % respectively. This confirms validity of the proposed EAF model.

2.5.2.3 VIC considering sinusoidal variation

Figure 2.41 shows comparison of VICs between the Cassie-Mayr's EAF model and the proposed EAF model under sinusoidal flicker condition. Identical variation in VIC confirms validity of the proposed EAF model.



(a)

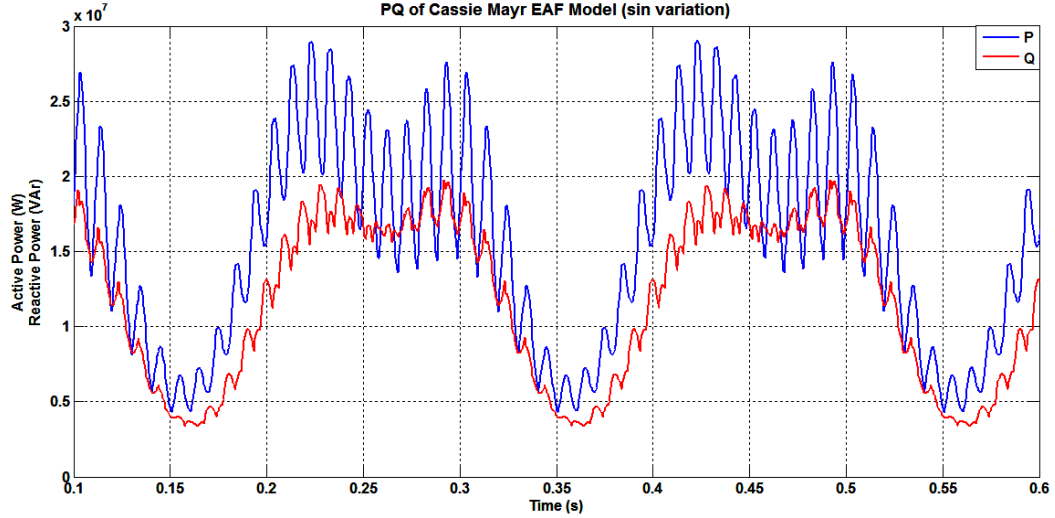


(b)

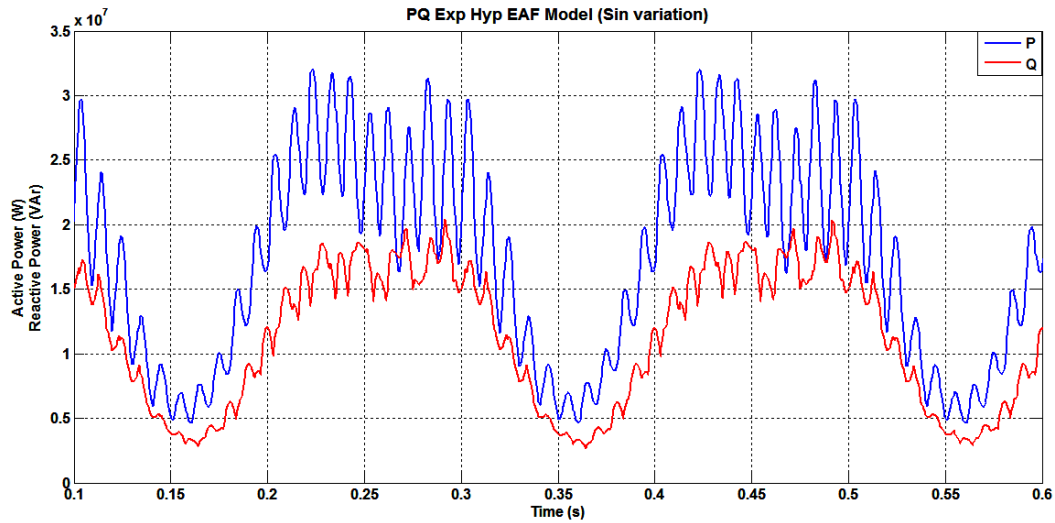
Figure 2.41 VIC of (a) Cassie-Mayr's EAF model (b) the proposed EAF model during melting cycle considering sinusoidal flicker

2.5.2.4 Active and reactive power (P-Q)

Figure 2.42 shows active and reactive power variation with reference to time. Similar variation pattern observed in P-Q consumption confirm validity of the proposed EAF model.



(a)



(b)

Figure 2.42 P-Q consumption of (a) Cassie-Mayr's EAF model (b) proposed EAF model during melting cycle considering sinusoidal flicker

2.5.2.5 Random variation

Mathematically the random variation can be expressed as [83], [90]:

$$v_{at}(t) = V_{at0} [1 + m \cdot N(t)] \quad (2.17)$$

$N(t)$ is expressed with zero mean and variance of one. Table 2.10 shows parameters used for random variation.

Table 2.10 Parameters for random variation

Parameter	Value
V_{at0} (V)	200
m	0.8
$N(t)$ (Hz)	4-14

Figure 2.43 shows MATLAB simulation of random flicker generation.

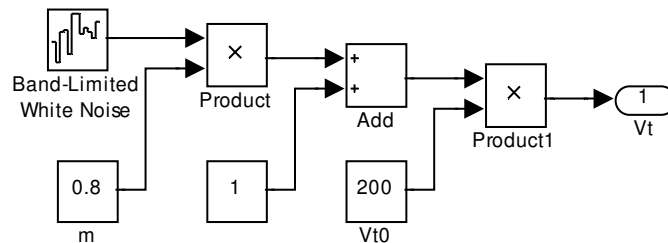
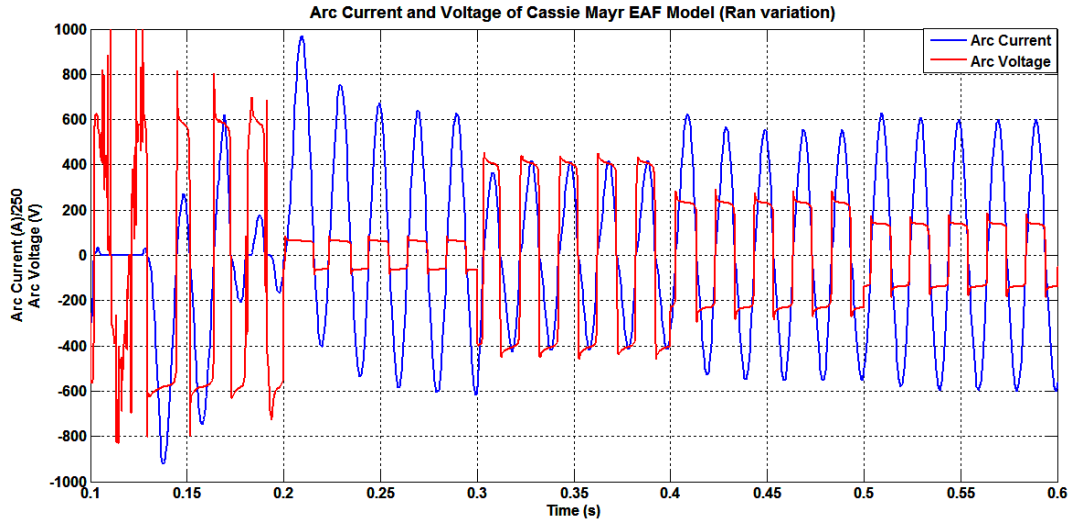


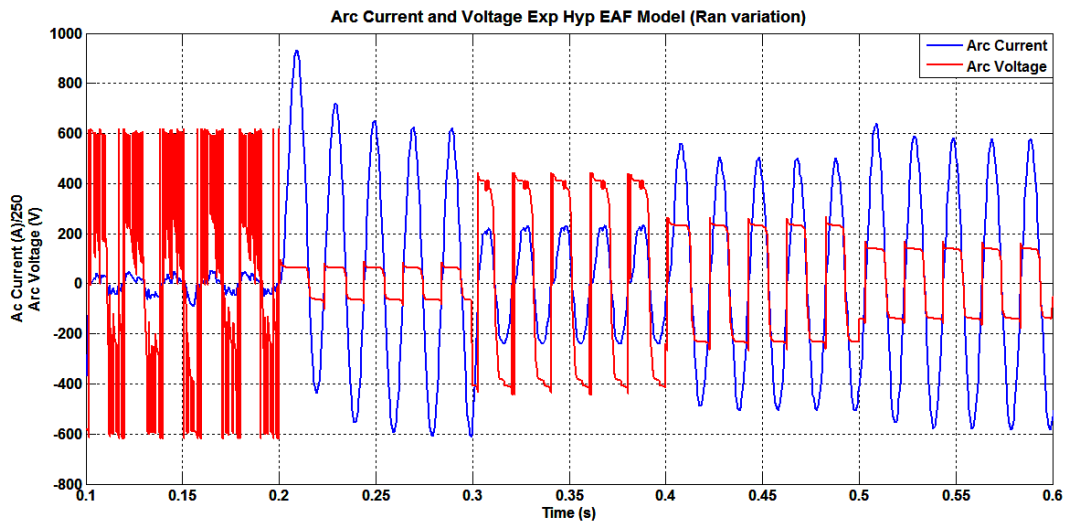
Figure 2.43 Simulink/MATLAB Simulation of random flicker generation

2.5.2.6 Arc current & arc voltage considering random variation

Figure 2.44 shows simulation results for random flicker.



(a)



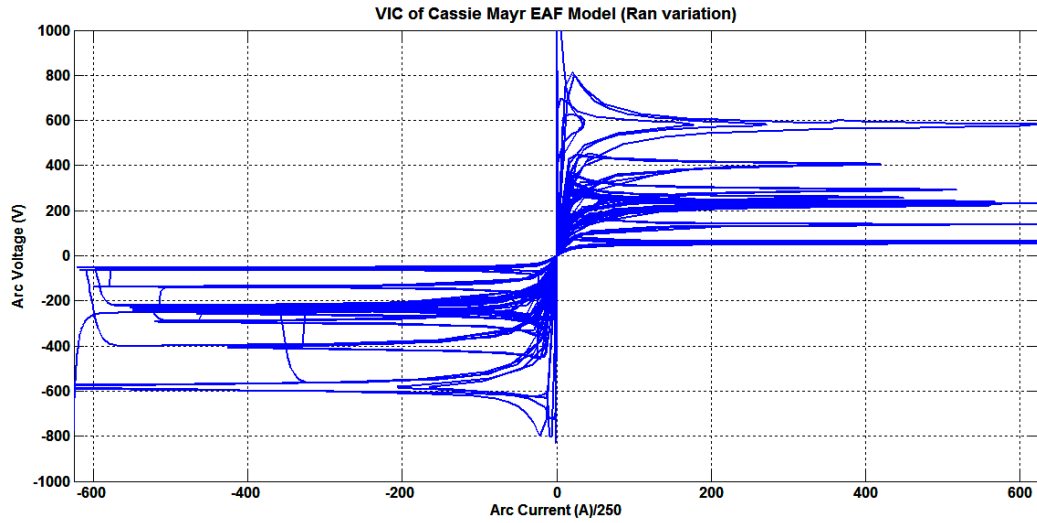
(b)

Figure 2.44 Waveform of arc voltage-current v/s time of (a) Cassie-Mayr’s EAF model (b) Proposed EAF model during melting cycle considering random flicker

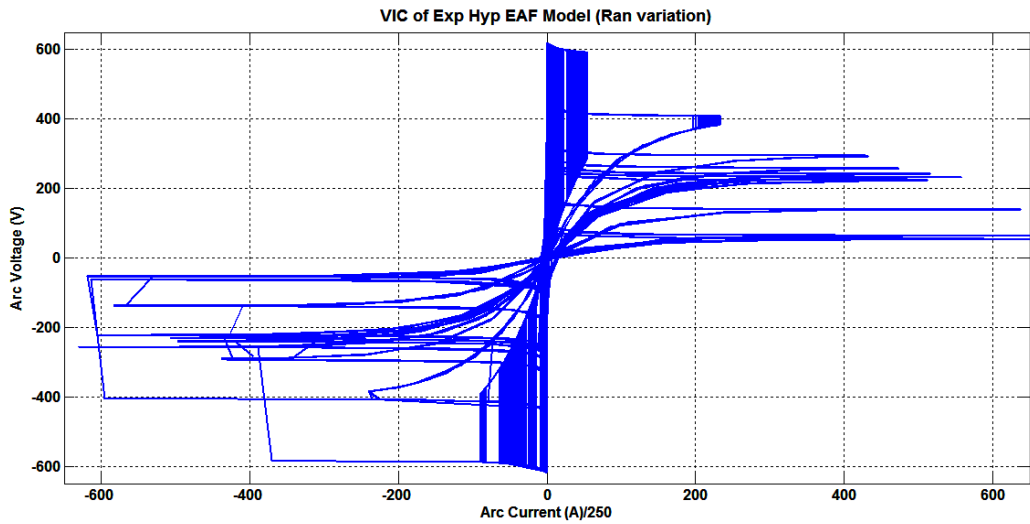
Variation in arc voltage and arc current during melting cycle (considering random variation) of the proposed EAF model is matching with close proximity to that of Cassie-Mayr’s EAF model. The real measured data in [94] also validates the same fact.

2.5.2.7 VIC considering random variation

Figure 2.45 shows comparison of VICs between the Cassie-Mayr's EAF model and the proposed EAF model under random flicker condition. Identical variation in VIC confirms validity of the proposed EAF model.



(a)



(b)

Figure 2.45 VIC of (a) Cassie-Mayr's EAF model (b) the proposed EAF model during melting cycle considering random flicker

2.6 EAF Distribution Network Simulation

In this study, the system of a realistic steel plant is under test to assess the harmonics and flicker as PQ issues in the EAF connected distribution network. Figure 2.46 shows the single-line-diagram of the test system. The steel plant is fed by a high-voltage transmission line of rating 110 kV. In order to provide an adequate voltage level to the arc furnace two step-down transformers are used. The arc furnace is connected to the utility through transformer T₁ (110/13.8 kV High-Voltage/Medium-Voltage) and T₂& T₃ (13.8/0.55 kV Medium-Voltage/Low-Voltage) as presented in the SLD of Fig. 2.46. Transformer T₄ and T₅(13.8/0.55 kV) are utilized to supply the auxiliaries of the EAFs.

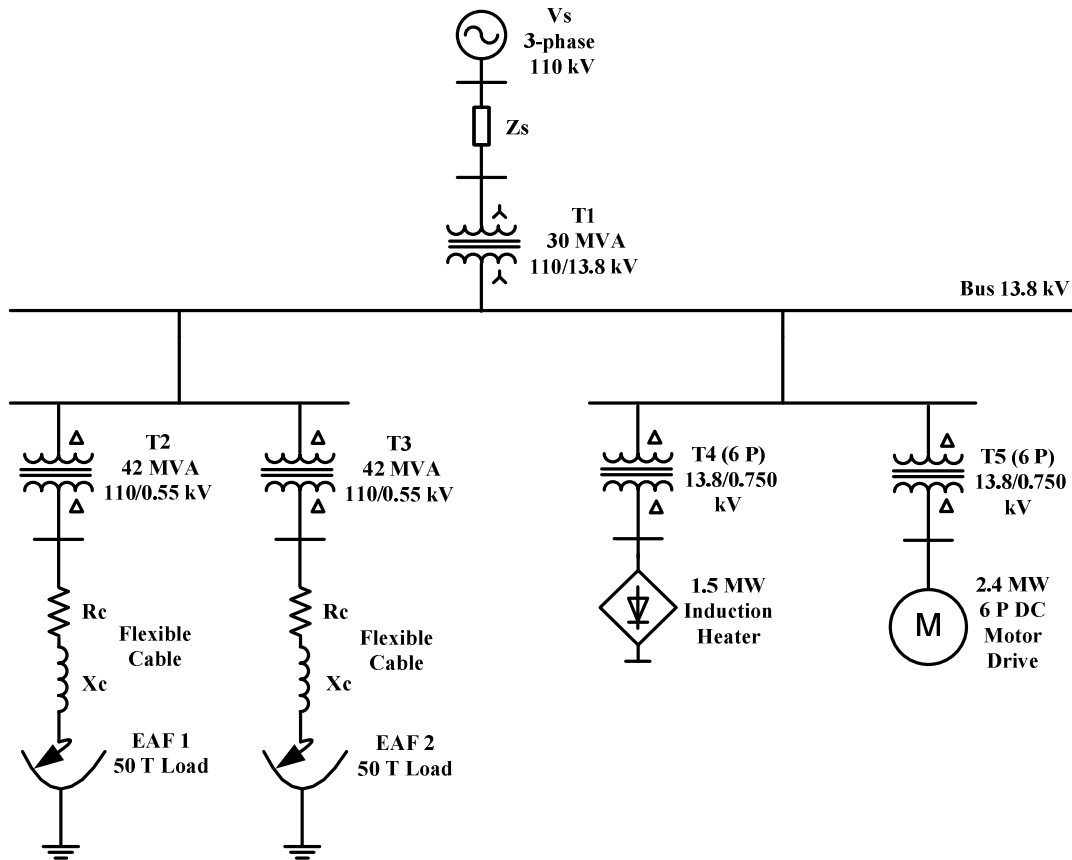
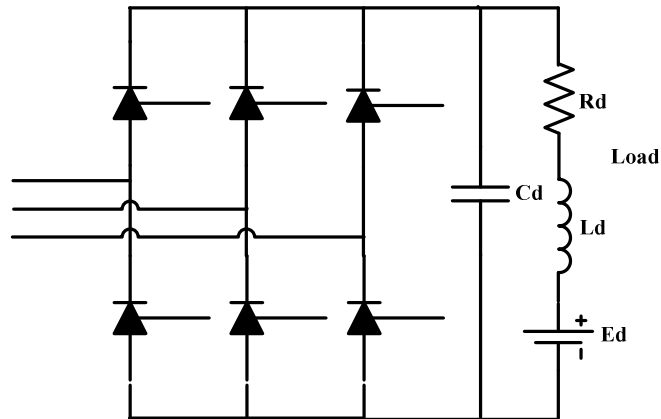


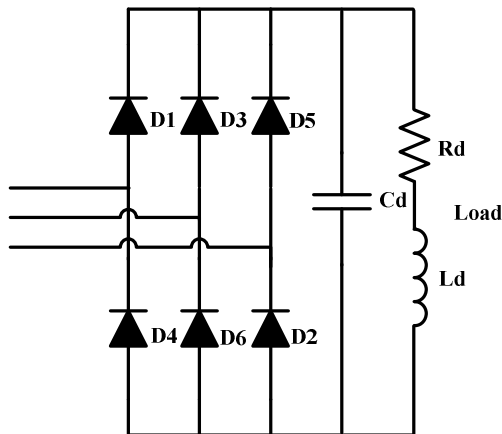
Figure 2.46 Single line diagram of test system

As shown in the Figure 2.46 the system consists of two electric loops: EAF and rolling mill (RM) loops. The EAF loop includes a 50-ton EAF load for steel making. The RM loop includes a bulk of DC rectifier and DC motor drive which are responsible for controlling the width and the thickness of the refined steel product.

Figure 2.47 (a) shows the circuit of the 6-pulse AC/DC thyristor-bridge rectifier for 6-pulse DC motor drives, where the motor load is modeled as equivalent impedance in series with a back-emf. The DC link capacitor is also connected to form a low-pass filter for reducing the ripple.



(a)



(b)

Figure 2.47 RM loop auxiliaries (a) equivalent 6-pulse DC motor drive (b) three-phase 6-pulse converter

The used six-pulse converter is modeled as uncontrolled diode-bridge converter, as shown in Figure 2.47 (b).

Table 2.11 lists the parameters associated with the motor drives. For the 6-pulse motor drive, a synchronized firing angle generator is modeled to trigger the thyristors with an equidistant firing scheme.

Table 2.11 Parameters of DC drive and converter

Drive/Converter	R_d (Ω)	L_d (mH)	C_d (μF)	E_d (V)	α ($^\circ$)
DC drive (2.5 MW)	0.126	0.16	1500	455	25.5
Converter	25	10	1500		

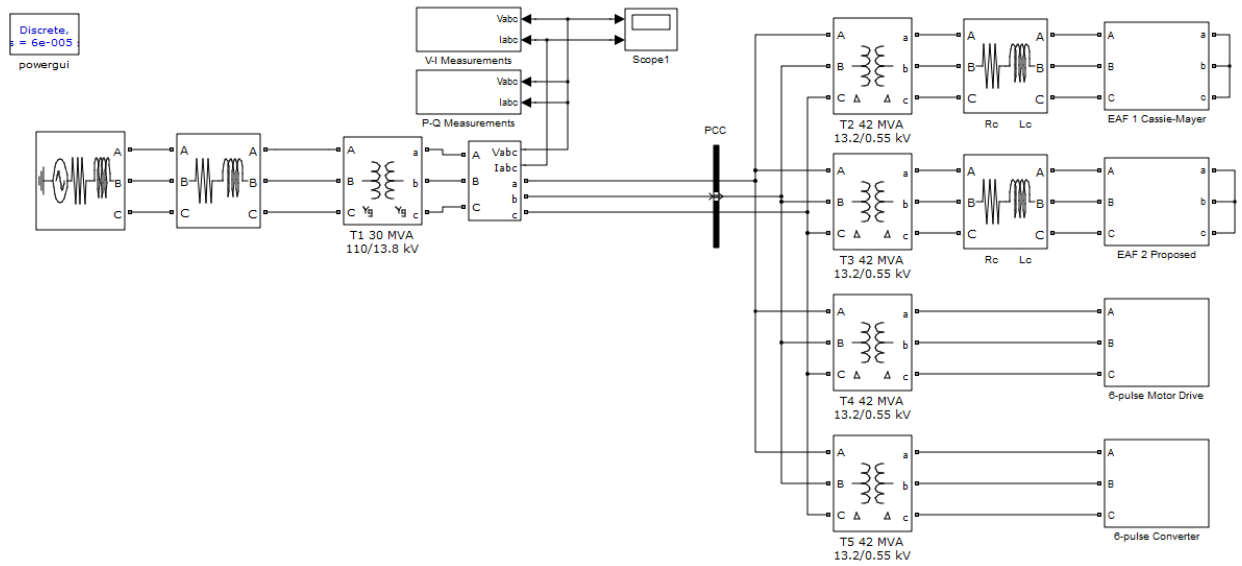
The system parameters along with the proposed EAF Model are tabulated in Table 2.12 [83]:

Table 2.12 Parameters of EAF distribution network

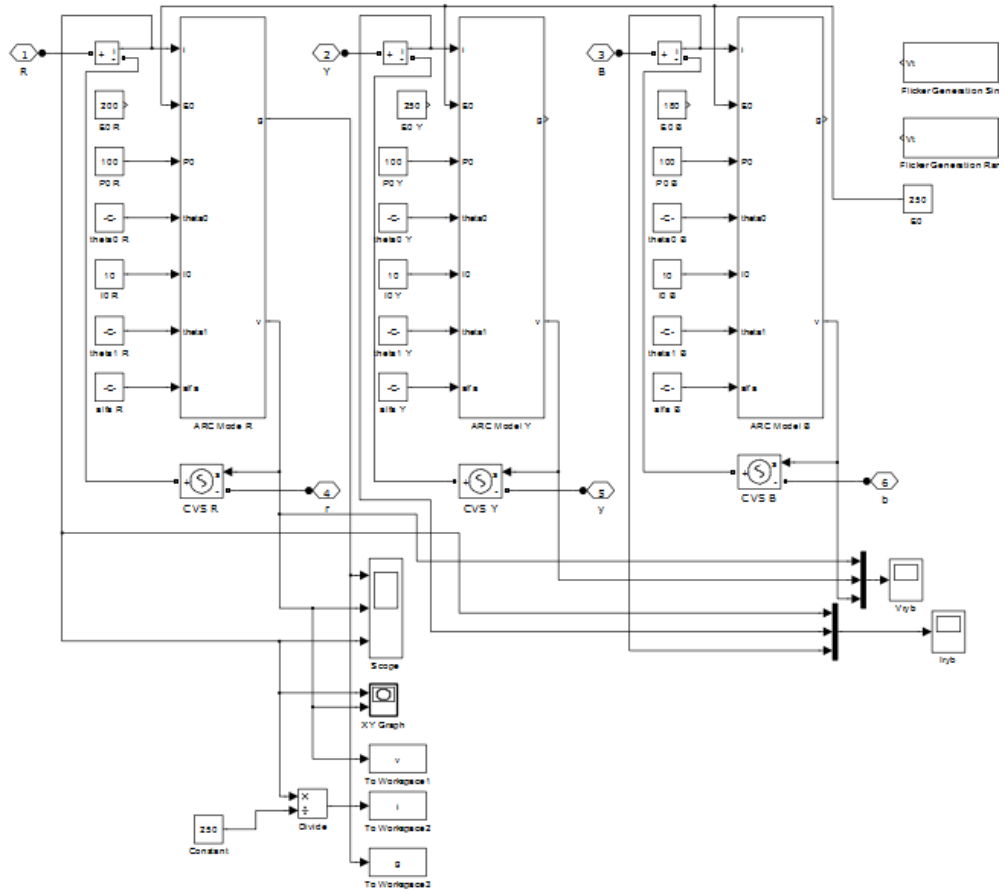
Parameters	Value
V (kV)	110
f (Hz)	50
Z_s (Ω /deg)	12.19 Ω /82.9
V_p / V_s of T1(kV/kV)	110/13.8
S of T ₁ (MVA)	30
V_p / V_s of T ₂ & T ₃ (kV/kV)	13.2/0.55
V_p / V_s of T ₄ & T ₅ (kV/kV)	13.8/0.750
S of T ₂ & T ₃ (MVA)	42
R_c (m Ω)	0.38
L_c (μ H)	8.589

The EAF along with the electric power system shown in Figure 2.48 is simulated using Matlab-Simulink platform to verify the proposed control. Each power device has been modeled using the SimPowerSystem toolbox library. Fig. 2.48 (a) shows complete Simulink/MATLAB file of EAF connected to the electric network. The distribution network consists of EAF-1-Cassie-Mayer model and EAF-2-Proposed model. Fig. 2.48 (b) shows

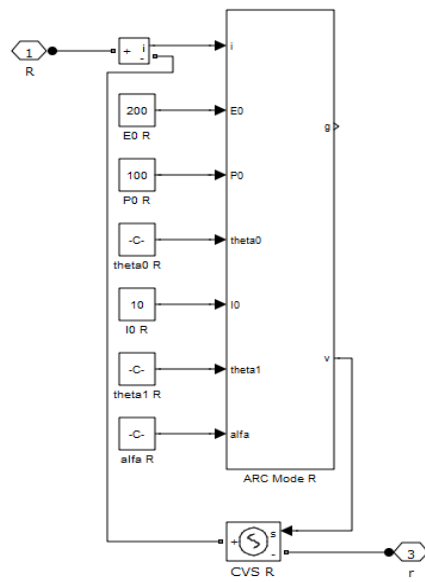
three simulated equation sets of Cassie-Mayer for three phases. As shown in Fig. 2.48 (c), EAF is modeled as a non-linear time varying voltage controlled source using subsystem/MATLAB. The arc current is taken as the input parameter to this function and the output is non-linear time varying voltage. Fig. 2.48 (d) describes detailed simulation of Cassie-Mayr's equations (2.3) to (2.5).



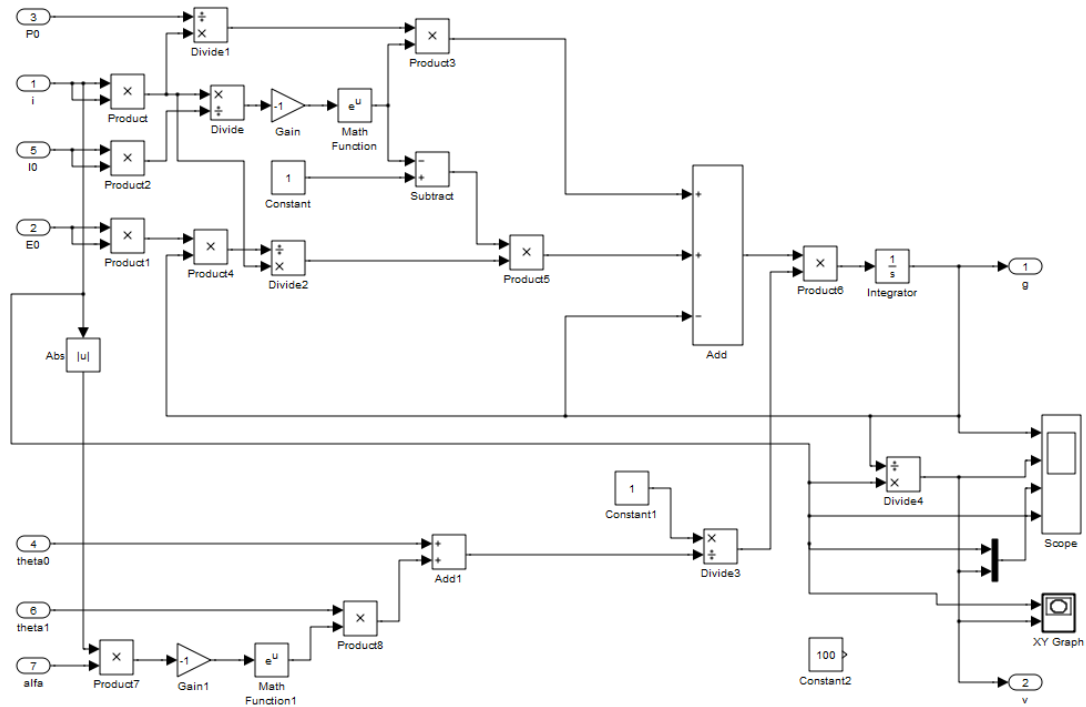
(a)



(b)



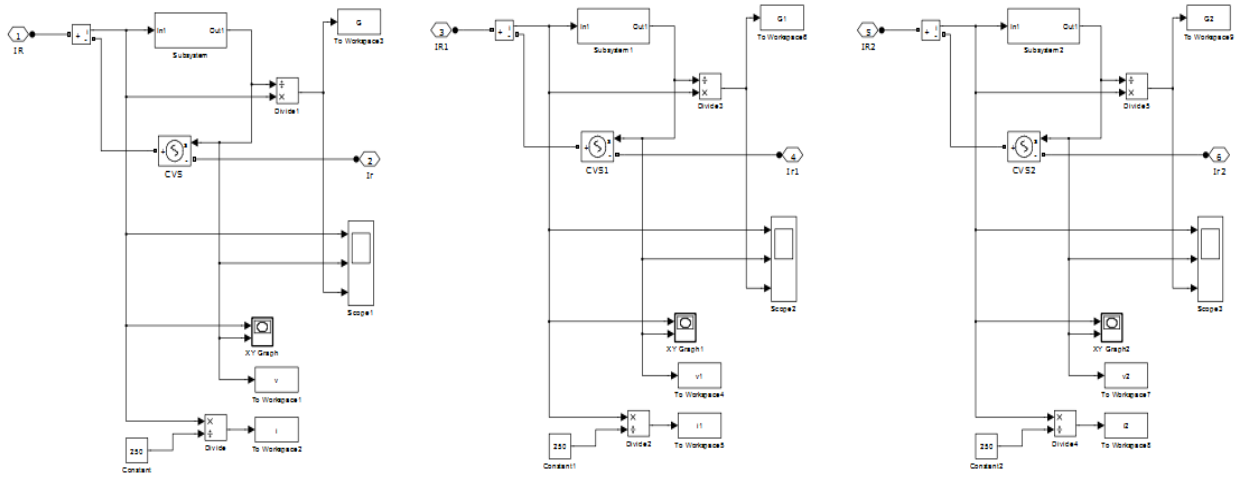
(c)



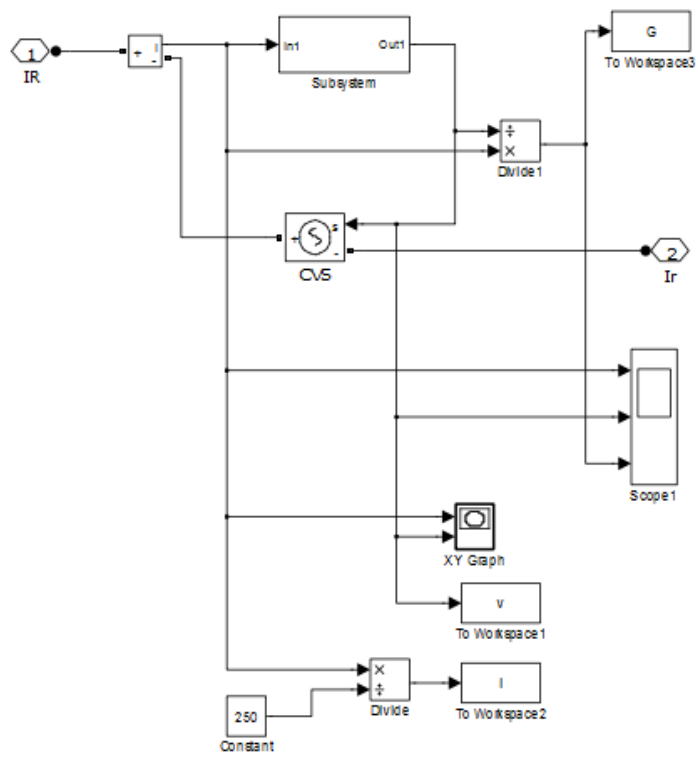
(d)

Figure 2.48 Complete Simulink/MATLAB simulation file of EAF Model 1 (Cassie-Mayer) (a) three phase network along with EAF (b) three phase EAF simulation (c) single phase EAF simulation (d) EAF equation simulation

Figure 2.49 shows simulation of proposed EAF model. Figure 2.49 (a) shows three simulated equation sets of the proposed EAF model for three phases. As shown in Figure 2.49 (b), EAF is modeled as a non-linear time varying voltage controlled source using subsystem/MATLAB. The arc current is taken as the input parameter to this function and the output is non-linear time varying voltage. Figure 2.49 (c) describes detailed simulation of the proposed model equation (2.10).



(a)



(b)

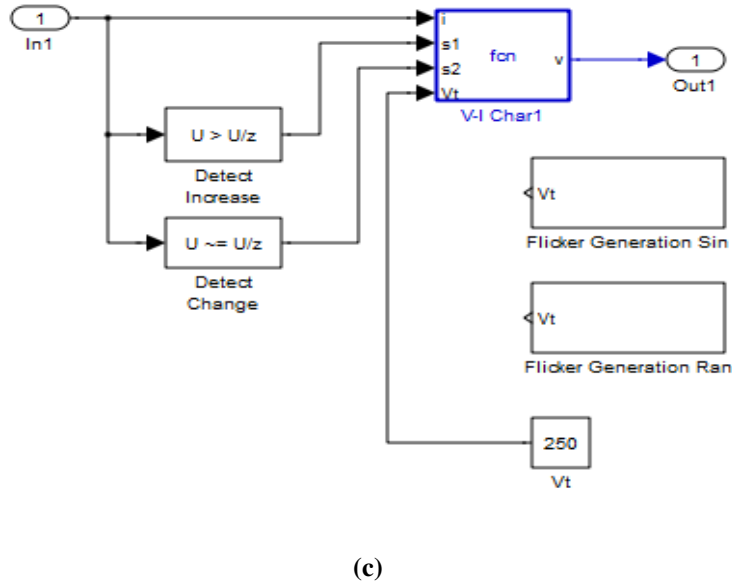


Figure 2.49 Complete Simulink/MATLAB simulation files of proposed EAF model (a) three phase network along with EAF (b) three phase EAF simulation (c) single phase EAF simulation

As shown in Figure 2.49 (c), the EAF is modeled as a non-linear time varying voltage controlled source using embedded program function/MATLAB. The arc current is taken as the input parameter to this function and the output is non-linear time varying voltage.

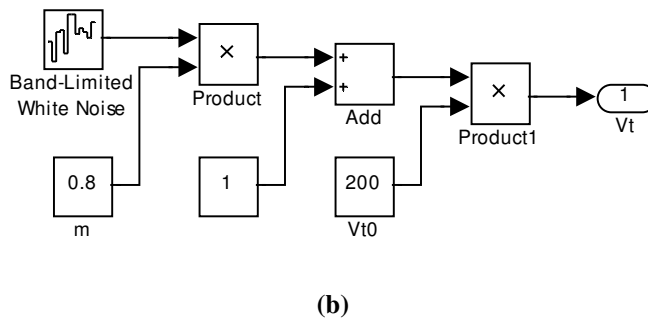
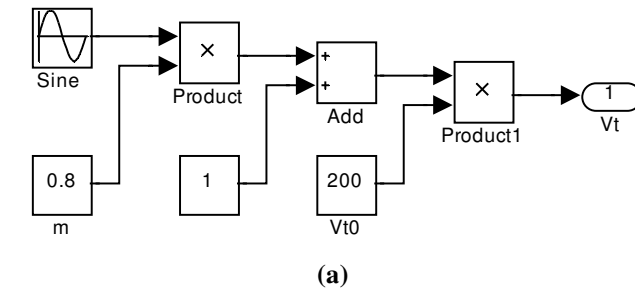
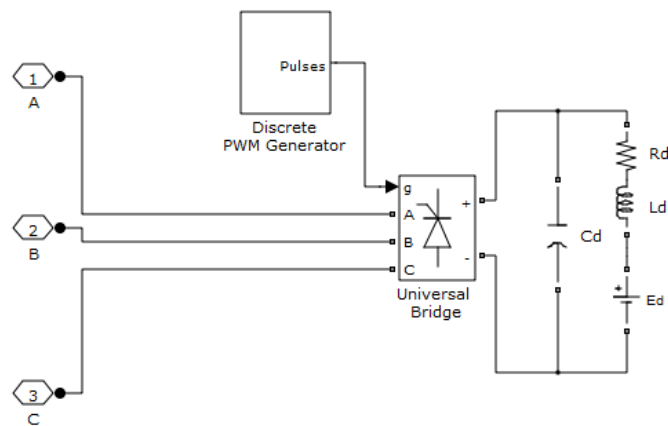


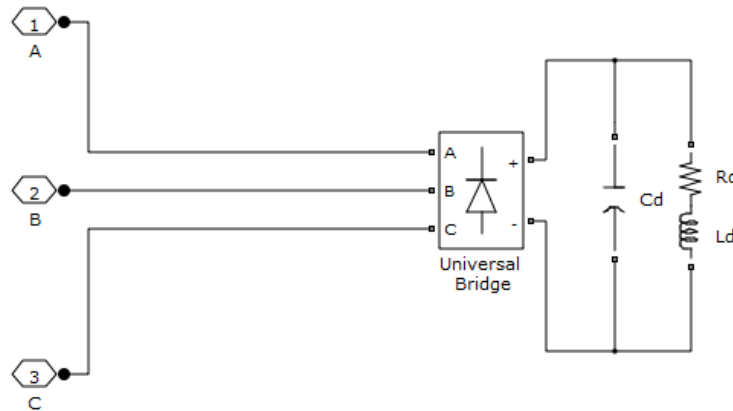
Figure 2.50 Simulink/MATLAB Simulation of (a) sinusoidal flicker (b) random flicker

Figure 2.50 (a) and (b) show simulation of equations (2.12) and (2.17) representing, sinusoidal and random flicker respectively.

Figure 2.51 shows Simulink/MATLAB simulation of RM auxiliaries shown in Figure 2.47. Figure 2.51 (a) shows the simulated circuit of the 6-pulse DC thyristor-bridge rectifier for 6-pulse DC motor drives, where the motor load is modeled as equivalent impedance in series with a back-emf. The DC link capacitor is also connected to form a low-pass filter for reducing the ripple. Figure 2.51 (b) shows simulation of three-phase six-pulse converter modeled as uncontrolled diode-bridge converter.



(a)



(b)

Figure 2.51 Simulink/MATLAB Simulation of (a) 6-pulse DC motor drive (b) three-phase 6-pulse converter

2.7 Summary

This chapter presents harmonic survey of various types of domestic as well as industrial loads. Practical measurement show that the THD_v for industrial loads is ranging from 0 % to 2.5 %, whereas for domestic loads is 2.1 to 4.33 %. Similarly, THD_i for industrial loads and domestic loads is ranging from 9.3 % to 50.83 % and 12 % to 96.94 % respectively. As discussed in the previous chapter, the limit imposed for maximum harmonic distortion by IEEE-519, 1992 is 5 % for both THD_v and THD_i . It can be seen that the industrial and domestic loads are satisfying IEEE limits for THD_v but exceeding limits for THD_i . EAF is chosen as an industrial load for simulating distribution network. A new time domain EAF model is proposed to study power quality problems. The proposed model is a combination of two previous EAF models called-exponential and hyperbolic model-using transition functions. The functioning of the proposed model has been validated by comparing its performance characteristics with the existing Cassie-Mayr EAF model. Simulation carried out in SIMULINK/MATLAB environment validates the proposed EAF model. The main features of the proposed EAF model are good mathematical approximation, no need of initial conditions, and no need of measurements in actual arc and consideration of unbalanced three phase currents. The proposed model can be used to describe various operating cycles of electric arc furnace and its impact on the connected electric network from power quality point of view. Finally, the proposed method presents a suitable model with a very good approximation for the VIC. The model is also able to describe the almost all the specifications of EAF. In this chapter, a three phase structure of the electric EAF is proposed which includes the power quality aspects-voltage harmonics, current harmonics, voltage flicker and unbalance loading. Two types of voltage flicker-sinusoidal and random-are carried out. Detailed power quality analysis is presented. The proposed novel EAF model is useful to study power quality issues pertaining to EAF connected distribution network, to design and to validate various power quality improvement techniques. Finally, EAF distribution network test model is constructed and simulated, which consist of EAFs along with the auxiliaries.